Fire Safety Journal 121 (2021) 103272

Contents lists available at ScienceDirect

Fire Safety Journal

journal homepage: http://www.elsevier.com/locate/firesaf

Development of a plug-and-play fire protection system for steel columns

Jérôme Randaxhe [a,b,*], Nicoleta Popa [a], Olivier Vassart [a], Nicola Tondini [b]

[a] Global R&D Center of ArcelorMittal, Esch-sur-Alzette, Luxembourg
[b] Department of Civil, Environmental and Mechanical Engineering, University of Trento, Italy

ARTICLE INFO

Keywords:
Steel structure
Fire protection
Standard fire
FE thermal Analysis
Rock wool board
Steel sheets

ABSTRACT

The paper presents the development of an innovative cost-effective fire protection system for steel columns, which is quick and easy to install and to dismantle. In terms of assembly, this protection is designed to be a plug-and-play system, which is made of two U-shaped half-protections that encapsulate a column. They are composed of high-density rock wool boards arranged in U-shape steel sheets presenting a system of claws to ensure their connection. Small-scale experimental tests were performed to evaluate the insulating efficiency of the system and the thermal behaviour of the connection claws. Numerical models were then developed with the finite elements software ABAQUS and SAFIR and were successively calibrated based on experimental results. Subsequently, full-scale experimental tests were performed according to the European standard of regulation EN13381-4 and the results certified that the fire protection is effective for steel profiles with section factor ranging from 42 to 103 m^{-1} to maintain the steel temperature below 550 °C when exposed to a standard fire for 120 min. Finally, a cost analysis was performed to attest the competitivity of the plug-and-play fire protection system by considering direct and indirect costs.

1. Introduction

1.1. Existing fire protection systems

Passive fire protection systems for steel structures have been investigated for decades. Their role is to delay the heating of structural components by isolating them from fire. In this respect, Islam et al. [1] studied the vulnerability of steel columns under the standard ISO 834 heating curve [2] through numerical analysis. Typically, existing fire protections are made of insulating materials which may be divided into three categories: intumescent paints, sprays and boards. Petukhovskaia [3] investigated and summarized passive fire protection methods for load-bearing structures in case of hydrocarbon fire. Leborgne and Thomas [4] illustrated three fire protection systems, i.e. intumescent paints, sprayed-based protections and board systems, and described their application with their advantages and limits. The National Institute of Standards and Technology (NIST) [5] reported an overview of existing fire protections for structural steel members with their advantages and disadvantages. Currently, almost all protections require important installation times on construction site, which represent costs and exposure to risks for technicians. A brief description of these fire protections is presented herein with their main characteristics.

An intumescent paint fire protection guarantees insulation efficiency for steel members by producing chemical reaction in event of fire. When heated to around 200 °C, an intumescent paint layer expands to form a layer up to 50 times thicker, which ensures the insulation of the member. The layer thickness to be applied depends on the targeted fire resistance. As depicted in Fig. 1a, paints offer a clean visual aspect. They can be applied by an off-site or in-site treatment depending on the project. In both cases, their proper application requires time and qualified labour which make these paints an expensive protection. Intumescent paints are suitable to protect complex structural connections and can be reused in case of building dismantlement. Lots of research is going on about intumescent coatings and its use in a performance-based fire engineering context when natural fire curves are used to investigate the structural fire behaviour. Lucherini and Maluk [6] reviewed intumescent coatings for the fire-safe design of steel structures. De Silva et al. [7] experimentally investigated steel elements protected with intumescent coatings. De Silva et al. [8] subsequently developed a procedure for modelling the intumescent coating in both simplified and advanced calculation methods based on experimental results. Griffin [9] modelled the heat transfer across intumescent polymer paints. Gardelle et al. [10] studied a silicon-based coating. Luangtriratana et al. [11] quantified the

* Corresponding author. Global R&D Center of ArcelorMittal, Esch-sur-Alzette, Luxembourg.
E-mail addresses: jerome.randaxhe@arcelormittal.com (J. Randaxhe), nicoleta.popa@arcelormittal.com (N. Popa), olivier.vassart@arcelormittal.com (O. Vassart), nicola.tondini@unitn.it (N. Tondini).

https://doi.org/10.1016/j.firesaf.2020.103272
Received 20 April 2020; Received in revised form 6 December 2020; Accepted 28 December 2020
Available online 2 January 2021

Nomenclature

A_p/V	nominal box section factor of steel profile [m^{-1}]
λ_{RW}	theoretical thermal conductivity of rock wool [W/mK]
c_{RW}	specific heat of rock wool [J/kgK]
ρ_{RW}	density of rock wool [kg/m^3]
w_{RW}	water content of rock wool [kg/m^3]
$\alpha_{c,hot}$	convection coefficient for hot surface [W/m^2K]
$\alpha_{c,cold}$	convection coefficient for cold surface [W/m^2K]
ε_{RW}	relative emissivity of rock wool [-]
E_c	Young modulus in compression of rock wool [MPa]
$c_{Num.i}$	calibration coefficient [-]
$\lambda_{Num.i}$	calibrated thermal conductivity of rock wool [W/mK]
λ_{avg}	average of $\lambda_{Num.i}$ [W/mK]
σ	standard deviation of $\lambda_{Num.i}$ [W/mK]
$\lambda_{\beta,50\%}$	50th fractile of the beta distribution of $\lambda_{Num.i}$ [W/mK]
d_p	thickness of the protection layer [m]
λ_p	thermal conductivity of the protection [W/mK]
c_p	specific heat of the protection [J/kgK]
c_a	specific heat of steel [J/kgK]
ρ_p	protection density [kg/m^3]
ρ_a	steel density [kg/m^3]
$\theta_g(t)$	gas temperature at time t [°C]
$\theta_a(t)$	steel temperature at time t [°C]
$\Delta\theta_g(t)$	gas temperature increase during Δt [°C]
$\Delta\theta_a(t)$	steel temperature increase during Δt [°C]
Δt	time step [s]
θ_a	design temperature [°C]
$\lambda_{\theta a}$	predicted thermal conductivity of rock wool for θa [W/mK]
a_i	regression coefficient [-]
$\Delta L_{Tot}(t)$	total axial displacement at time t [mm]
$\Delta L_{Therm.}(t)$	thermal expansion at time t [mm]
$\Delta L_{Mech.}(t)$	mechanical axial displacement at time t [mm]
$T(t)$	overall mean temperature of loaded profile at time t [°C]
T_0	overall mean temperature of loaded profile at time t = 0 [°C]
α	thermal expansion coefficient of steel [$°C^{-1}$]
L	height of loaded profile [m]
k	correction factor [-]
t_l	time for loaded specimen to reach design temperature [min]
t_1	time for unloaded specimen to reach design temperature [min]
t_c	corrected time for unloaded specimen to reach design temperature [min]
S	box section factor for loaded steel profile [m^{-1}]
S_1	box section factor for unloaded steel profile [m^{-1}]
D	protection thickness for loaded steel profile [m]
D_1	protection thickness for unloaded steel profile [m]
b_i	regression coefficient [-]
b_i'	modified regression coefficient [-]

thermal barrier efficiency of intumescent coatings. Chen et al. [12] studied the performance of ultrathin intumescent paint for steel plates at elevated temperature. Mariappan [13] reviewed the recently developed intumescent coatings for structural steel. These numerous studies were encouraged by the increase of the market demand for intumescent paints in the past decade.

Sprayed-based fire protections can have different chemical compositions; as for example, they can be cementitious, gypsum, and vermiculite based. These products must be directly sprayed on structural members on site. The thickness to be sprayed also depends on the targeted fire resistance. Although the spray application is rapid, it is wet and requires a drying period which can delay the construction site progress. In fact, an area where a structure is being sprayed cannot be occupied by other workers. As depicted in Fig. 1b, the spray visual aspect suits only very low frequented areas, for instance basements and car parks. Sprays offer the advantages to cover complex structural geometries and to be a low-cost solution, but they cannot be easily reused in case of building dismantlement. Fulmer [14] developed and patented a cementitious spray without using any adhesive. Zhang and Li [15] recently developed a spray adopting engineered cementitious composite technology to address durability issues.

Fire protections made of boards can be made of gypsum, wood, or

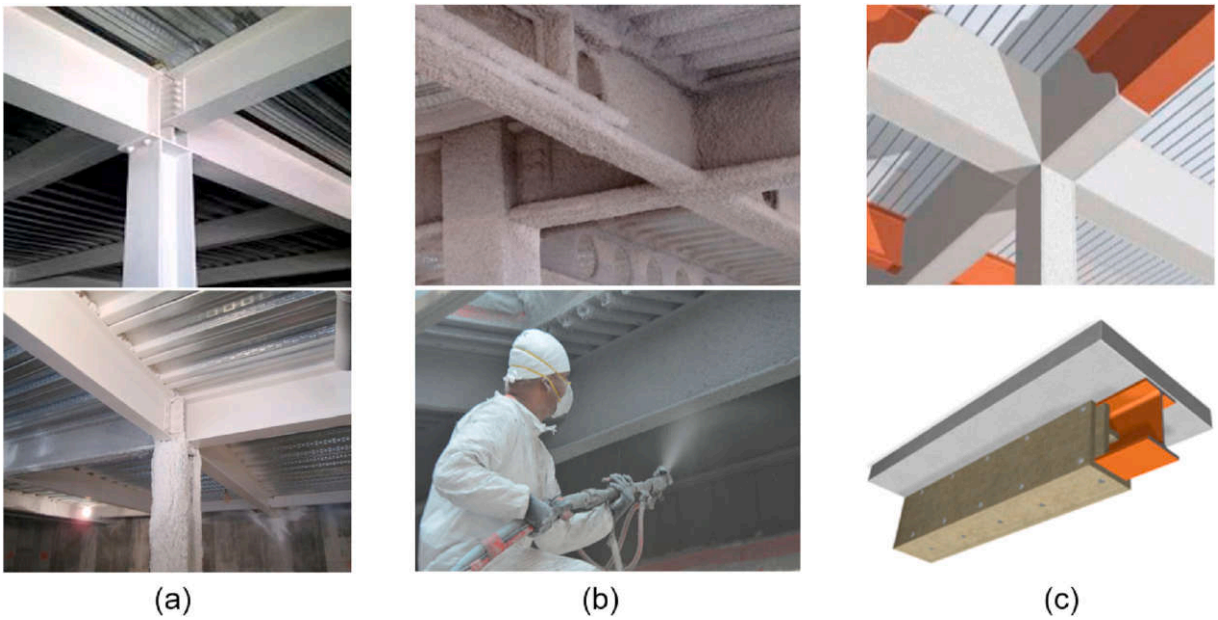

Fig. 1. Existing fire protection systems: a) Intumescent paints; b) Sprays; c) Boards.

any other rigid insulating material such as rock wool. Protecting structural members with board requires a tailor-made installation on site. Boards need to be cut, attached to members with screws or glue and eventually finished to offer a good visual aspect if required. This is a time-consuming process. Even though boards can be made of cheap materials, they are usually an expensive solution due to the labour cost. As depicted in Fig. 1c, when made of gypsum, boards solutions present a clean visual aspect which can suits any sort of building occupancy. However, that is not the case for all boards, as for example the ones made of rock wool that must be subsequently covered to prevent contacts with users as they can be irritating for the skin. Globally, board systems used as fire protections for steel columns also benefit from research conducted in the development of fire resistance wall panels usually made of rock wool, mineral wool or gypsum. Zhang et al. [16] studied the fire resistance of tubular steel columns protected with gypsum boards, rock wool boards and blanket made of alumina-silica materials. Keerthan and Mahendran [17] numerically studied gypsum plasterboard panels under standard fire. Gottfried [18] developed and patented a board system to wrap structural steel members and made of several layers of insulating material. Zago and Keiser [19] patented a rigid protection system composed of different components, made of gypsum boards surrounded by a steel sheet, to be screwed together. Different metallic connectors were conceived to equip steel profiles flanges extremities and provide attaching surface to screw fire resistant gypsum boards. Parker [20] developed and patented a first version of such connectors and Ramos [21] developed and patented an alternative and continuous version of these connectors.

Considering existing fire protection systems, Akaa et al. [22,23] proposed an analysis technique to select the optimal system based on structural performance and cost criteria. Lim et al. [24] used numerical analysis to evaluate the performance of passive fire protections in processing facilities. Existing fire protection systems differ in their global cost, installation process and visual aspect, although they all delay the heating of structural steel members. Obviously, fire protection visual aspect is correlated with costs and depends on the construction type and the architectural aesthetics that is being sought. Good visual aspects usually require higher costs. However, the key disadvantage shared by these systems remains the time required for their installation. The application of these fire protections must be all undertaken on construction sites, except for the intumescent paints when applied off-site. This observation raises two questions: cost and safety. The direct costs of a fire protection system are the ones related to materials and labour. The indirect costs are related to maintenance and are generated within construction projects due to the installation time of the fire protection. The latter, in particular, can be significant in terms of delay, damage, or accessibility limitations for other workers. Regarding the safety, it is well known that construction sites are areas more exposed to risks and hazards than familiar environments such as manufacturing plants. It means that with a fire protection system that requires long installation delay, the exposure to risk for the installation technicians increases because workers must spend more time on site. Considering these two aspects, it seems relevant to develop an innovative fire protection system that addresses installation time issue, which intertwines costs and safety. Indeed, especially with current construction sites where the numbers of subcontractors and their interactions can be very important, it is in the community interest to design a safer and cost-efficient fire protection system. Furthermore, in order to maximise its cost efficiency, it is also important to consider maintenance requirements in terms of time and costs.

1.2. Scope of the work

The scope of this work is to develop an innovative fire protection system for steel columns exposed to the standard fire by maintaining their temperature below 550 °C for 120 min. At 550 °C steel retains 62.5% of its strength and it can be deemed as a limiting temperature in a simplified approach for which the loads in the fire situation can be taken as 0.65 of the loads at the Ultimate Limit States as for EN 1993-1-2 [25].

The system is designed to protect steel columns with H, I and hollow square sections. It aims at simultaneously offering the advantages of the existing protection and to address their issues related to cost and safety. Therefore, the design of such a system started with the definition of the specifications to be fulfilled by the fire protection. Among these specifications listed in Table 1, the most innovative one is the plug-and-play connection system which facilitates short installation time and dismantlability. Indeed, the fire protection system must innovate in terms of installation ease and rapidity. The dismantlability aspect aims at meeting the sustainability criteria that current projects have sometimes to fulfil when submitted for tender process. It has to be noted that the fire protection system was designed to protect steel columns exposed to fire on four sides. Therefore, the system has not been yet tested to protect steel columns exposed to fire on less than four sides, steel beams and structural connections. Since, in principle it can be used in combination with other fire protections systems the appropriateness of boundary conditions at the top and at the bottom of the protection system were also investigated in this work.

The work investigated all these aspects: fire performance and cost effectiveness.

The paper is organised as follows: Section 2 describes the design of the fire protection system based on the specifications and on small-scale experimental tests. Section 3 reports the outcomes of small-scale experimental fire tests conducted on seven columns equipped with different fire protections. Section 4 presents the numerical models that were developed to analyse the behaviour of the protection when exposed to the standard fire curve. Section 5 reports the implementation of large-scale experimental tests and the methodology prescribed by the standard of regulation EN13381-4 [26]. For that purpose, five specimens, presenting different section factors, were protected by the same fire protection system. Section 6 analyses the thermal data obtained from the large-scale experimental tests and assesses the thermal efficiency of the protection. This assessment follows a method defined by the standard of regulation leading to the certification of the fire protection. Design recommendations are also provided. Section 7 details a cost analysis of the developed fire protection and compares it with other protection systems based on direct and indirect costs. Finally, Section 8 draws conclusive remarks along with future perspectives.

2. Design of an innovative fire protection system for steel columns

The two key-elements of the fire protection development were the selection of the components and the design of the connection system. In the case of sprays and paints, there is no proper fixing system since the insulating material is self-fixing on structural members. For systems made of boards, it is essential to use a reliable fixing system. Boards may be highly insulating, but if their fixations fail, their insulating effect is significantly decreased, as highlighted by Wang and Li [27] who studied fire resistance of steel columns when fire protection is partially damaged.

Table 1
Fire protection specifications.

- "plug & play" system
- appropriate for steel columns exposed to fire on four sides
- appropriate for I, H and hollow square section types
- R120 fire resistant
- effective for columns exposed to standard fire for 120 min by maintaining steel temperature below 550 °C
- composed by 2 elements
- quick to install and dismantlable
- light enough to be manipulated by two workers
- cost-effective
- aesthetic

First, to ensure the fire resistance of the protection itself for 120 min, it was imperative to use non-flammable materials. Secondly, to facilitate a rapid installation on site, the insulating system had to be light and rigid enough to be manipulated with ease by two technicians. Especially for structural members presenting important heights, it was more convenient to deal with rigid components than smooth ones, such as blankets. To provide rigidity- and non-flammable aspects within the protection, it was decided to use high density rock wool boards and steel sheets. Nowadays, rock wool boards are already used as a fire protection system [28], but they require installation delay and aesthetic finishing. They are attached to steel structural members with glue or with specific pins directly welded on the member through the board. The use of steel sheets brings both rigidity and clean visual aspect to the protection.

Additionally, steel sheets can ensure its own connection system. As depicted in Fig. 2, the fire protection is made of two identical half-protections, prefabricated with steel sheets and rock wool boards. Steel sheets are formed with a U shape inside which high density rock wool boards are positioned with glue. The extremities of the steel sheets are specifically bent like claws to generate the connection system of the protection. The connections are made of two complementary claws, male and female, clasping into each other to bond the two half-protections. When the protection is properly installed around a column, the rock wool boards are against the column, which ensures its insulation and maintains the connection claws clasped into each other. Furthermore, this connection system is designed to present a safe behaviour against thermal dilation effects. When a protected column is exposed to heat, the two-half protections can freely expand while the claws remain connected. This is shown in Section 4.1. with 3D thermo-mechanical analyses. The installation of the two half-protections and their connection requires the application of forces as depicted on Fig. 3. When half-protections are installed around a column, rock wool boards are compressed against the flange of the profile and against each other while the claws push and slide along each other (Fig. 3b). Once the relative displacement of the claws is adequate, the claws can clasp into each other (Fig. 3c). It appeared that forces to be applied for the proper installation of the protection were very high. Therefore, clamps were used as tools to apply the appropriate pressure without impacting the protection integrity. However, the development of a more convenient tool could be the scope of future works.

Eventually, this plug-and-play system can be considered as a board system since its thermal efficiency is ensured with rock wool boards. The innovative aspect remains in the connection system generated by the steel sheets surrounding the boards. The use of steel sheets constitutes three advantages: I) it combines an easy assembling method; ii) a pre-manufactured system and iii) aesthetic aspects. Fig. 4 illustrates two pictures of the fire protection applied around a 3-m high column. The main objectives and features resulting from the fire protection design are outlined below.

1) The issue of thermal bridges at the connection level was carefully considered in the design. Therefore, the use of intumescent joint and the discontinuous set of rock wool boards inside steel sheets were contemplated options that are investigated in Section 3. Discontinuities within the global insulation thickness in the protection corners and at connection levels are illustrated in Fig. 2.
2) Both male and female claws ensuring the protection connection were designed to be continuous all along the height of the protection. However, considering important column height, it requires a

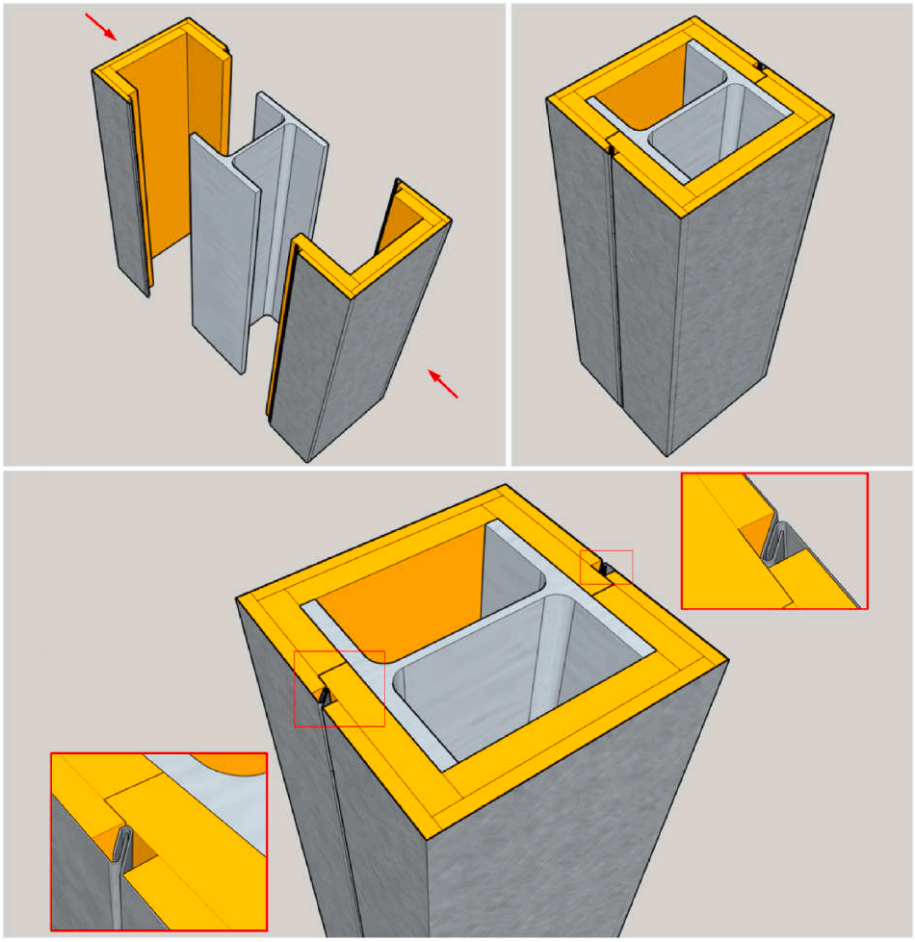

Fig. 2. Description of the fire protection: HEB240 protected with 45 mm of rock wool.

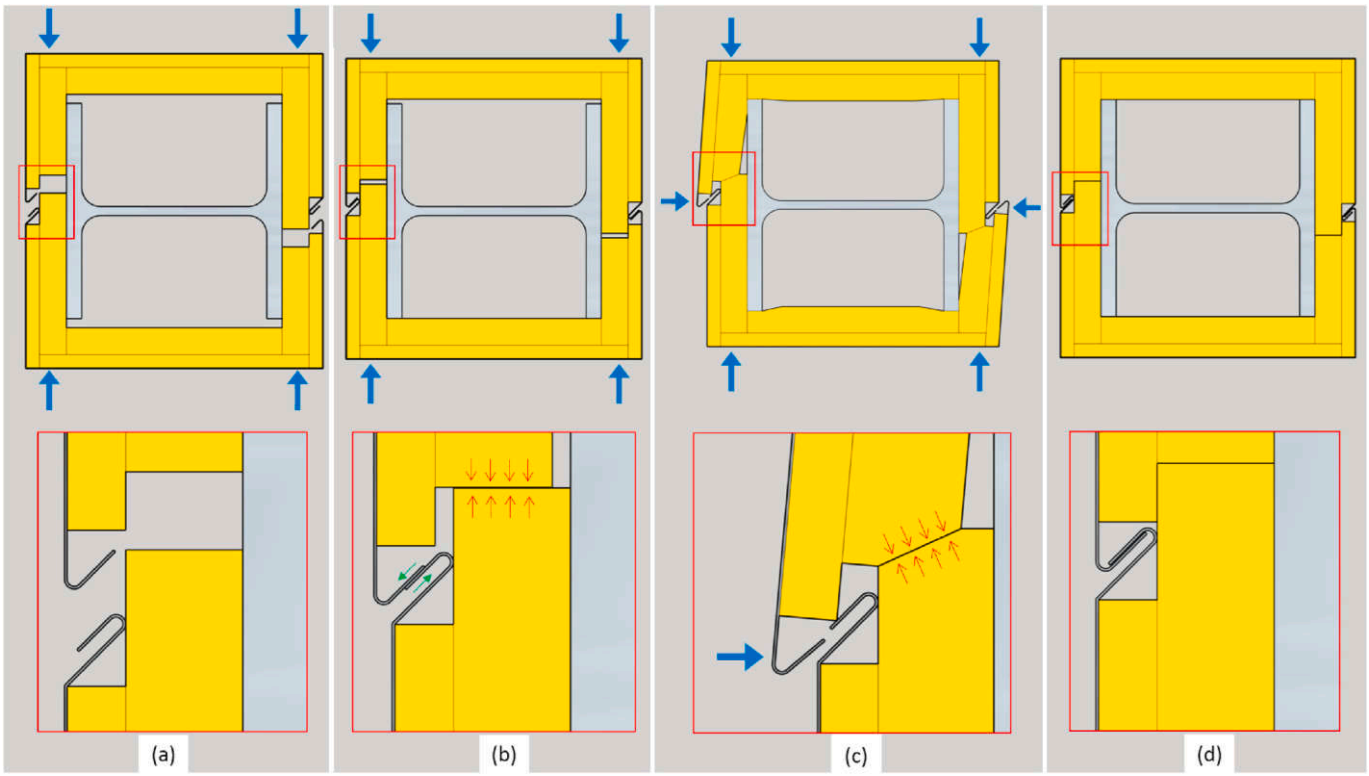

Fig. 3. Installation of the fire protection with a plug-and-play system.

Fig. 4. The plug-and-play system protecting a 3-m high column.

perfectly synchronised installation to permit the clasp all at once along the entire height. Since such installation appears complex to perform, it was decided to make the male claw discontinuous to allow a connection process like a zip connection, from the bottom to the top, as illustrated in Fig. 5.

3) The connection claws were designed with an angle of 45° that allows ease of connection and mechanical resistance. For aesthetic concerns, claws were bent inside the protection which represents an obstacle for the rock wool board. Thus, there are two options for the rock wool boards layout: i) rock wool boards are cut to perfectly fit the shape the claws; ii) rockwool board are cut with rectangular cross-section which reduces manufacturing costs but generates holes around connection claws. Both options and their thermal impact are investigated with in Section 3.
4) Finally, regarding the steel sheet thickness to be used and the length to be assigned to the connection claws, a good compromise between thermo-mechanical efficiency, protection weight and costs had to be

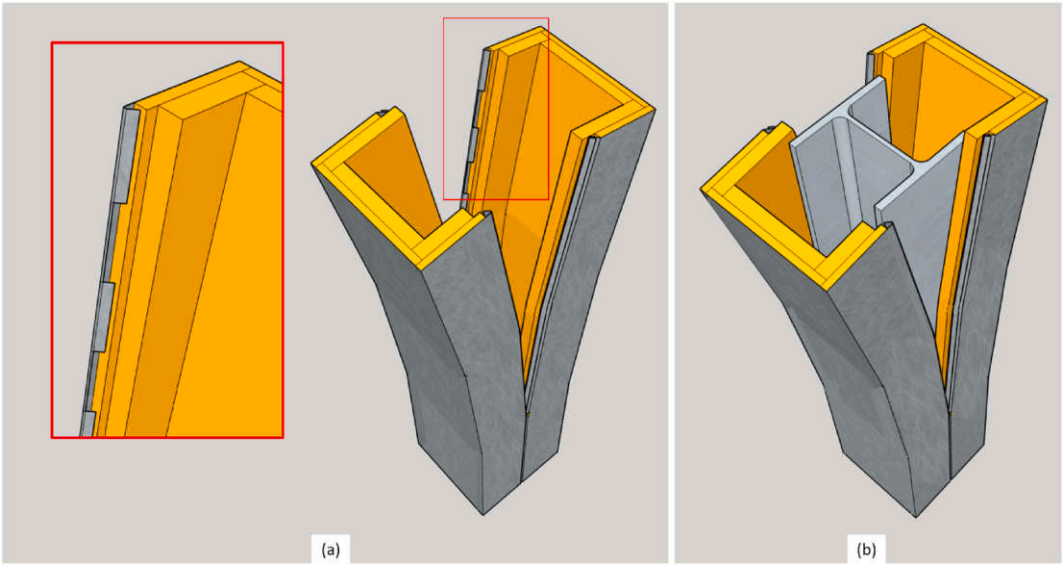

Fig. 5. Installation concept: a) Discontinuity of the male claws; b) Connection of two half protections around a steel profile.

found. Therefore, different thicknesses and lengths are evaluated experimentally in the next Section.

3. Small-scale experimental tests

3.1. Specimens and instrumentation

Seven small-scale experimental fire tests were performed at the research centre of metallurgy (CRM) in Liège, Belgium. The ISO 834 standard heating curve was applied to the specimens [2]. Small-scale tests took place along with the design phase of the fire protection to simultaneously improve its development and to evaluate its thermal efficiency. The geometries of the seven specimens are depicted in Fig. 6, where distinctive characteristics can be observed within the different specimens. As explained in Section 2, these tests aimed at evaluating different design features and options. Thus, between Specimen 1 and Specimen 7, modifications were made to the fire protection. As illustrated in Fig. 6, main modifications regard: intumescent joint; rock wool boards discontinuity at connection levels and within corners; discontinuity of male claws; holes at connection levels; steel sheet thickness and length of the connection claws. The properties of the seven specimens are summarized in Table 2. For Specimens 2, 3 and 4, the intumescent joint was made of an intumescent material that foams up pressure-free, forming a firm and heat-resistant foam in case of fire [29]. The scale of these experimental tests is considered as "small" due to the dimensions of the experimental furnace. Indeed, Fig. 7a depicts the experimental furnace with a cubic volume of 0.512 m^3 (0.8 m × 0.8 m x 0.8 m) and a square opening at the ceiling level of 0.04 m^2 (200 mm × 200 mm). Six specimens were inserted vertically in the furnace through the top opening and were therefore limited by its dimensions. They were HEB140 and HEB100 steel profiles respectively protected with 30 mm and 50 mm of rock wool, so that they sealed the opening by their own (Fig. 7b). Specimen 7 was shorter and inserted laterally in the furnace by the front door, while the top opening was sealed with ceramic fibre (Fig. 7c). It was a HEM220 steel profile protected with 45 mm of rock wool. Therefore, since the cross-section of Specimen 7 was larger than the opening at the ceiling level, its length had to be limited to 0.7 m. Furthermore, this specimen also served as a test to check the suitability of the boundary conditions to be used in the large-scale experimental campaign. In any case, the height of the specimens exposed to fire was limited to 0.8 m. As described in Fig. 8, the seven specimens were instrumented in the same way, with 14 thermocouples. 7 thermocouples were located at 200 mm from the bottom while the 7 other ones were positioned at 60 mm. They were welded on the profile, at mid-web, mid-flange and at the extremities of the flanges. As indicated in Fig. 8b, when specimens were inserted through the top opening, steel

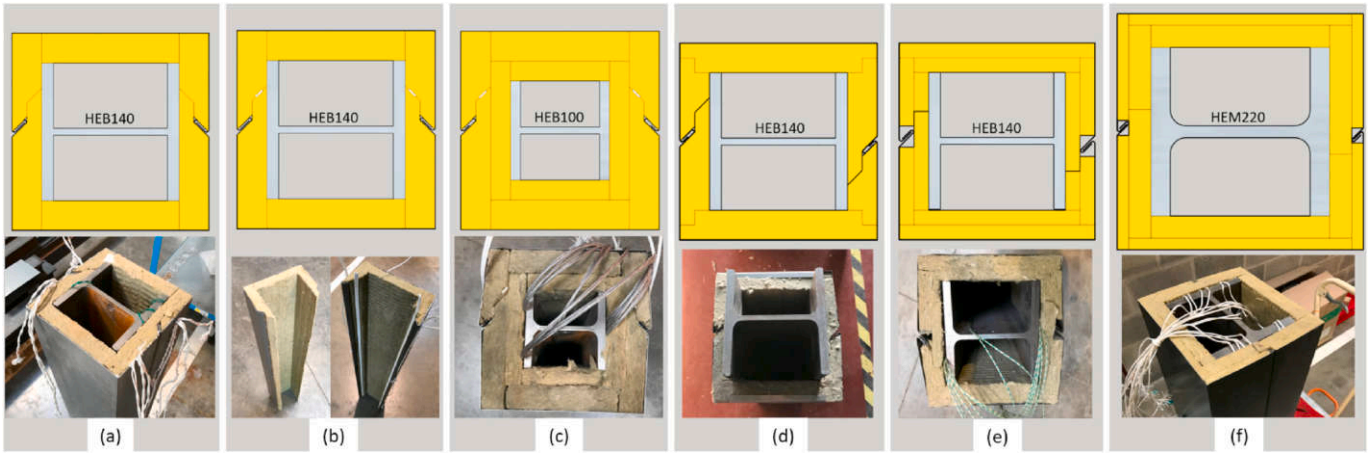

Fig. 6. Description of the small-scale experimental tests: a) Specimen 1; b) Specimens 2 and 3; c) Specimen 4; d) Specimen 5; e) Specimen 6; f) Specimen 7.

Table 2
Properties of the small-scale experimental tests.

Specimen	Profile	Box section factor A_p/V [m^{-1}]	Rock wool thickness [mm]	Steel sheet thickness [mm]	Discontinuity of the claws	Length of the claws [mm]	Identical half-protections	Hole at the connection level	Intumescent joint
1	HEB140	134	30	1	No	12	No	No	No
2	HEB140	134	30	1	No	12	No	No	Yes
3	HEB140	134	30	1	Yes	12	No	No	Yes
4	HEB100	161	50	1	Yes	6	No	No	Yes
5	HEB140	134	30	0.5	Yes	8	Yes	No	No
6	HEB140	134	30	0.5	Yes	12	Yes	Yes	No
7	HEM220	64	45	0.5	Yes	12	Yes	Yes	No

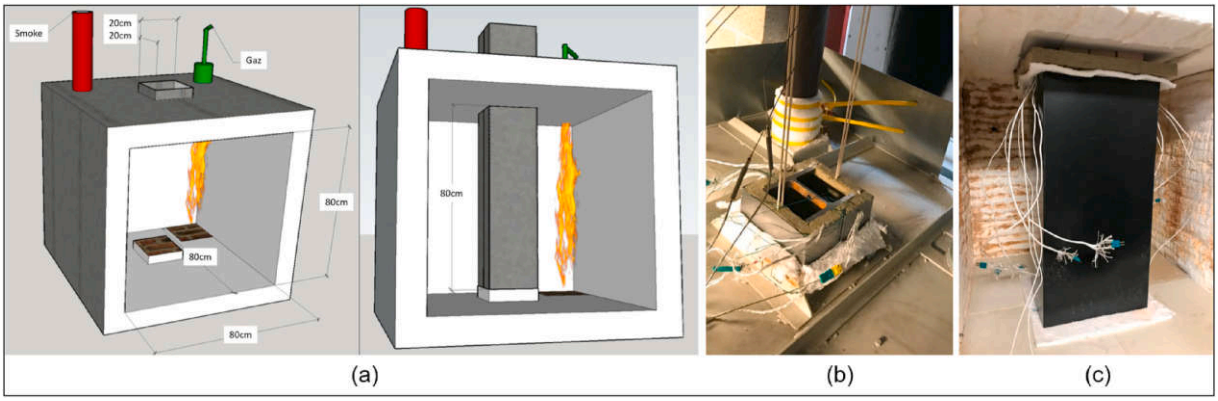

Fig. 7. Small-scale experimental furnace: a) Dimensions of the furnace; b) HEB140 inserted through the top opening; c) HEM220 inserted through the door.

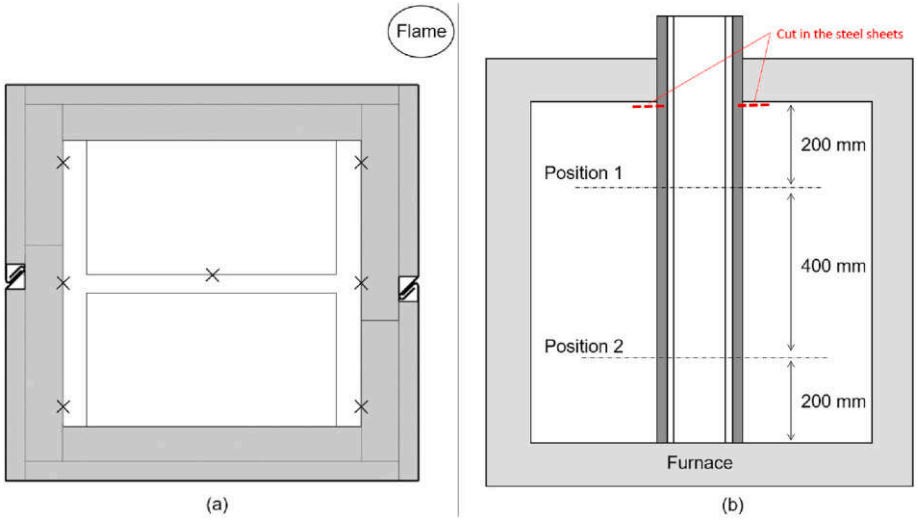

Fig. 8. Thermocouple locations: a) Plan view; b) Transversal view.

sheets were cut at the ceiling level of the furnace to reproduce realistic boundary conditions.

3.2. Experimental observations and results

For each of the seven specimens, the mean steel temperature evolution with time recorded by thermocouples positioned at 200 mm and 600 mm, are depicted in Fig. 9. For all of them except for Specimen 7, it was observed that thermocouples located at 200 mm recorded more severe temperature evolutions than thermocouples located at 600 mm. That is due to the fact that for Specimens 1 to 6, the top opening of the furnace was sealed by the specimen itself. Thus, that could constitute a cooling source for the specimens, which explains such thermal gradients. Collecting all the curves on the same graph, Fig. 9 shows that Specimens 1, 2, 3, and 5, all having almost the same geometry, followed similar temperature evolutions during the whole test. They reached steel temperatures very close to 725 °C after an exposure of 120 min to the standard fire. By comparing Specimens 1, 2 and 3, that are endowed with similar characteristics (see Table 2), the use of an intumescent joint at the connection claw level appeared not necessary. Specimen 1 presented a lower temperature evolution with time than Specimens 2 and 3, as it reached a temperature of 709 °C after an exposure of 120 min to the standard fire, against 719 °C and 726 °C for Specimens 2 and 3, respectively. Based on that observation, it was decided not to use an intumescent joint in the protection system composition. Specimen 4 presented an abnormally high temperature evolution, which was

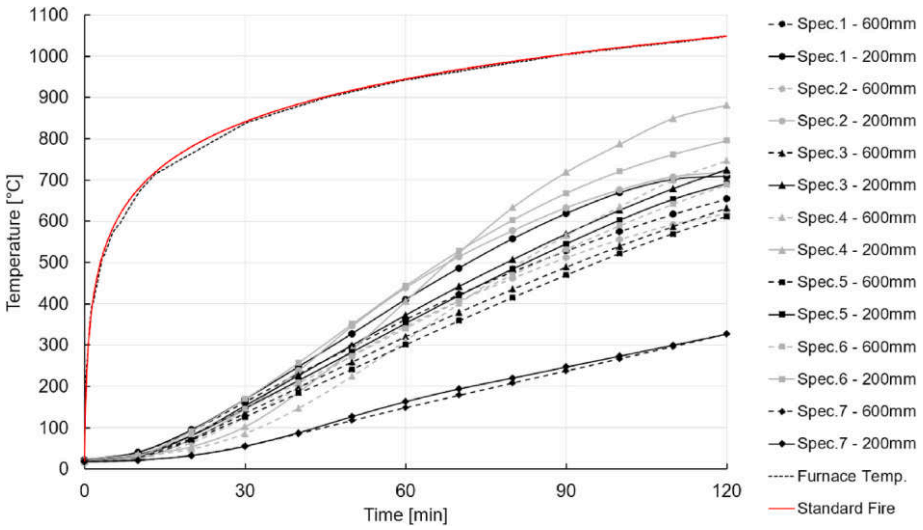

Fig. 9. Small-scale experimental test results – Mean temperatures recorded at 200 mm and 600 mm.

unexpected according to the numerical predictions based on theoretical values (see Section 4.2). Thermocouples located at 200 mm recorded temperatures reaching 882 °C after 120 min. They were attributed to thermal bridges due to manufacturing imperfections. Specimen 6 presented temperature evolution close to the ones observed with Specimens 1, 2, 3 and 5 during the first hour of test, whereas during the second hour, Specimen 6 reached the temperature of 795 °C. This could be explained by the presence of holes at the levels of the connection claws, which constituted thermal bridges, since the rock wool thickness was reduced to 15 mm. Specimen 7 followed temperature evolution with time significantly lower than other specimens. After an exposure to the standard fire of 120 min, Specimen 7 reached the temperature of 327 °C. That was expected due to the lower section factor of the profile and the 45-mm thick insulation layer. Since the furnace was completely closed, there was during the first hour of test only a small thermal gradient between thermocouples at 200 mm and 600 mm due to the flame orientation. After 120 min of exposure to standard fire, the mean temperatures recorded at 200 mm and 600 mm were identical. Considering these observations, the most severe mean temperatures recorded at 200 mm were used as the basis for the conservative calibrations of the numerical models developed in Sections 4.2. Although different lengths of the claws were tested (6 mm, 8 mm and 12 mm), Fig. 10 shows that the seven protection systems remained well connected and closed around the steel profiles during the 120 min of exposure to standard fire.

4. Numerical and analytical models

This section aims at developing numerical and analytical models allowing for a proper understanding of the thermo-mechanical behaviour and the thermal efficiency of the fire protection. However, it is important to underline and keep in mind that both experimental tests, numerical and analytical models present sources of uncertainty, as mainly quantified in Section 5.4 for the large-scale tests.

In the experimental field, the conditions in which a test is performed can present uncertainties on many aspects. Considering the test of a fire protection system, these aspects can refer to the integrity of the system, the regularity of an insulating layers, the presence of thermal bridges, or also the proper set up of the thermocouples.

In numerical and analytical methods, the model of a fire protection system is usually developed with perfect geometries that neglects the uncertainty related to the actual geometry of the components. Moreover, without available experimental values, the thermal properties of the materials are taken as the nominal ones. 2D thermal analyses that are only performed on the cross sections of steel profiles can also be source of uncertainty without considering the heat transfer occurring along the longitudinal axis of the structural member.

In order to properly quantify the sources of uncertainty raised hereabove, the strategy adopted in this work was to calibrate the thermal conductivity value characterising the protection system, by considering more severe thermal conductivity values in the numerical

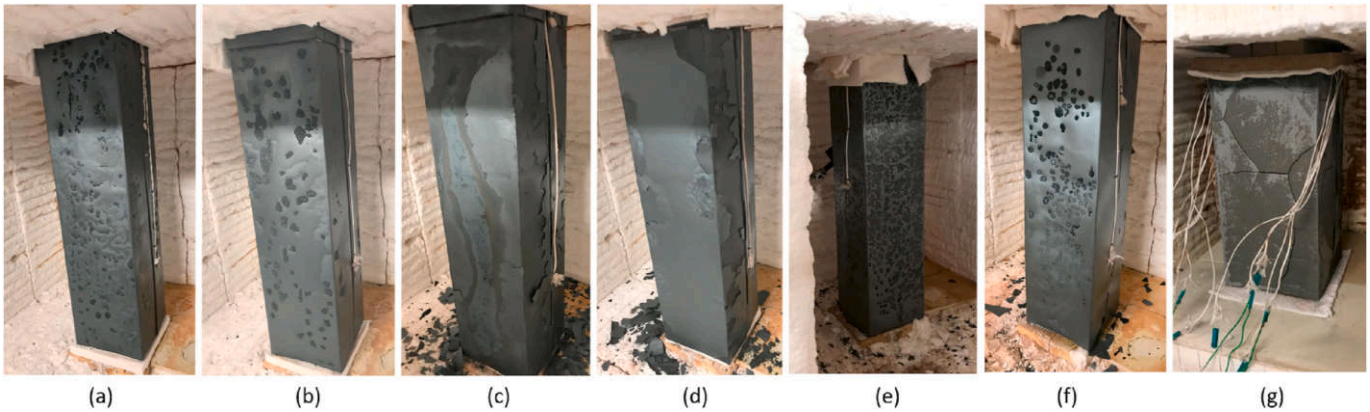

Fig. 10. Specimens after the 120 min of exposure to standard fire: a) Specimen 1; b) Specimens 2; c) Specimen 3; d) Specimen 4; e) Specimen 5; f) Specimen 6; g) Specimen 7.

and analytical models. In this way, it was possible to achieve conservative results against experimental observations.

4.1. 3D numerical model

A 3D numerical model was created with the software ABAQUS [30] to study the thermo-mechanical behaviour of the protection. More specifically, the aim of this model was to analyse whether or not the connection claws could disconnect due to steel sheet thermal expansion. Therefore, dynamic implicit procedure was adopted to perform nonlinear analysis. An HEB140 steel profile, protected with 30 mm of rock wool and a 1 mm thick steel sheet, was exposed to standard fire for 120 min. The steel profile, the rock wool boards and the steel sheets were modelled with five components discretised with coupled temperature-displacement 3D solid elements, i.e. C3D8T elements [30], using a mesh size of 5 mm. Thermal and mechanical properties of steel, varying with temperature, were defined as prescribed in EN1993-1-2 [25]. Thermal and mechanical properties of rock wool were considered independent of temperature and were provided by the supplier [28] and are summarized in Table 3. The thermal conductivity value of rock wool boards was taken as a constant with temperature and equal to 0.2 W/mK. Thanks to the symmetry of the protection and the thermal loading condition, being the standard temperature-time curve uniformly applied all around the steel sheet, the analysis could be limited to half a model. For that purpose, appropriate boundary conditions were defined at the symmetrical axis level, as depicted on Fig. 11a. The steel profile was fixed along the six directions at the web extremity to stabilize the entire model. The rock wool boards and the steel sheets were free to move vertically but were fixed along the five other directions. Appropriate interactions were defined between the different components to represent the real conditions and geometrical constraints of the protection system. “Tie” constraints were defined between rock wool and steel sheets components; i.e. nodes defining both components and presenting identical coordinates were forced to displace conjointly. “Hard contact” interactions were defined between steel sheet components and between rock wool and steel profile components; i.e. components can displace independently but constitute obstacles which prevent them from compenetrating. As illustrated in Fig. 11b and c, the five components thermally expanded after 120 min of exposure to standard fire. As expected theoretically, the protection thermal expansion was more important than the one of steel profile (up to 2.2 mm compared to 0.8 mm), since they were subjected to a thermal gradient of 1000 °C. The two steel sheets displaced relatively to each other, but their claws remained connected. The connection system of the fire protection was designed to present a safe behaviour when heated, so that the thermal expansion of the protection does not tend to disconnect the claws but to keep them closed. This numerical investigation allowed the assessment of this thermal effect. This model reproduced the behaviour of the protection observed with small-scale experimental tests and depicted in Fig. 10 where specimens remained all well connected around profiles after 120 min of exposure to standard fire. In a first attempt, this 3D model was developed with a height of 10 mm to reduce the calculation demand. Since it provided satisfying results, its height was increased up to 100 mm and subsequently up to 300 mm. However, no differences were observed, such as steel sheet buckling or claws opening. Therefore, the thermal expansion of the fire protection should not significantly affect the claws connected all along the height of the protected column.

Table 3
Thermal and mechanical properties of rock wool.

Properties	Symbol	Value	Unit
Thermal conductivity	λ_{RW}	0.20	[W/mK]
Specific heat	c_{RW}	968	[J/kgK]
Density	ρ_{RW}	160	[kg/m^3]
Water content	w_{RW}	1.00	[kg/m^3]
Convection coefficient for hot surface	$\alpha_{c,hot}$	25.0	[W/m^{2}K]
Convection coefficient for cold surface	$\alpha_{c,cold}$	4.00	[W/m^{2}K]
Relative emissivity	ε_{RW}	0.80	[-]
Young modulus in compression	E_c	0.55	[MPa]

4.2. 2D numerical model

2D numerical models were created with the finite element software SAFIR [31] and calibrated against experimental results to quantify the fire protection thermal efficiency. For that purpose, each specimen cross-section, including the steel profile and the surrounding protection, was discretised with triangular finite elements using a mesh size of 6 mm. These models allowed the accurate geometrical reproduction of the seven specimens and the comparison between experimental- and numerical thermal results. The 2D numerical model corresponding to Specimen 6 is, for instance, depicted in Fig. 12a, where the standard temperature-time curve was applied all around the protection. In the same way as for the 3D numerical model, thermal properties used for the rock wool are the ones summarized in Table 3 and thermal properties of steel are taken from EN 1993-1-2 [25]. Fig. 12b illustrates the temperature field in Specimen 6 after 120 min of exposure to standard fire. The graph depicted in Fig. 13a shows, for each Specimen, the maximum temperature evolution observed in the cross section. Maximum temperatures obtained numerically are intentionally compared with average temperatures observed experimentally to subsequently calibrate numerical models in a conservative way.

For Specimens 1, 2, 3, 4 and 6, numerical predictions based on theoretical values provided lower temperature evolutions with time than experimental ones. Between numerical predictions and experimental tests, temperature differences of −14 °C, −24 °C, −32 °C, −286 °C and −85 °C were respectively observed for Specimens 1, 2, 3, 4 and 6. It means that the numerical model underpredicted the temperature by −2%, −3%, −4%, −32% and −11% for Specimens 1, 2, 3, 4 and 6, respectively. This can be explained by the thermal dilatation of the protection which is not considered in this numerical model and by manufacturing imperfections of the specimens. Indeed, imprecision in the board cutting could generate thermal bridges at some points. For Specimen 5, numerical predictions appeared to coincide fairly well with experimental results. A temperature difference of only +2 °C, i.e. +0.4%, was observed between the numerical prediction and the experimental test. For Specimen 7, although the presence of holes around the connection claws, the numerical prediction provided a more conservative temperature evolution with time than the experimental one, i.e. + 38 °C (+32%). That can be linked to its lower section factor and its higher protection thickness.

In order to take into account these differences between numerical predictions and experimental results, the rock wool thermal conductivity (TC) value was calibrated for each specimen with a coefficient $c_{Num.i}$. To calibrate this parameter was convenient since it has a direct influence on the protection thermal efficiency. For each specimen i, the theoretical TC value λ_{RW} was multiplied by the proper coefficient $c_{Num.i}$, as defined in Eq. (1), so that numerical models provided more conservative (or more optimized for Specimen 7) temperature evolutions with time than experimental ones. It has to be noted that, since the system developed here was designed to protect steel columns for 120 min, coefficients $c_{Num,i}$ were defined based, for each of the 7 specimens, on experimental temperatures observed after 120 min of exposure to the standard fire. This is illustrated on the graph in Fig. 13b. For each specimen, the coefficients $c_{Num.i}$ and the corresponding calibrated TC values $\lambda_{Num.i}$ are listed in Table 4.

$$\lambda_{Num.i} = c_{Num.i} . \lambda_{RW} \quad [W/mK] \tag{1}$$

After the calibration process, it can be observed from Fig. 13b that the numerical predictions are now close to the experimental evolutions in time of the steel temperature. In particular, this is true for five out of the seven small-scale experimental, while two of them presented significantly higher temperature evolutions with time in order to match

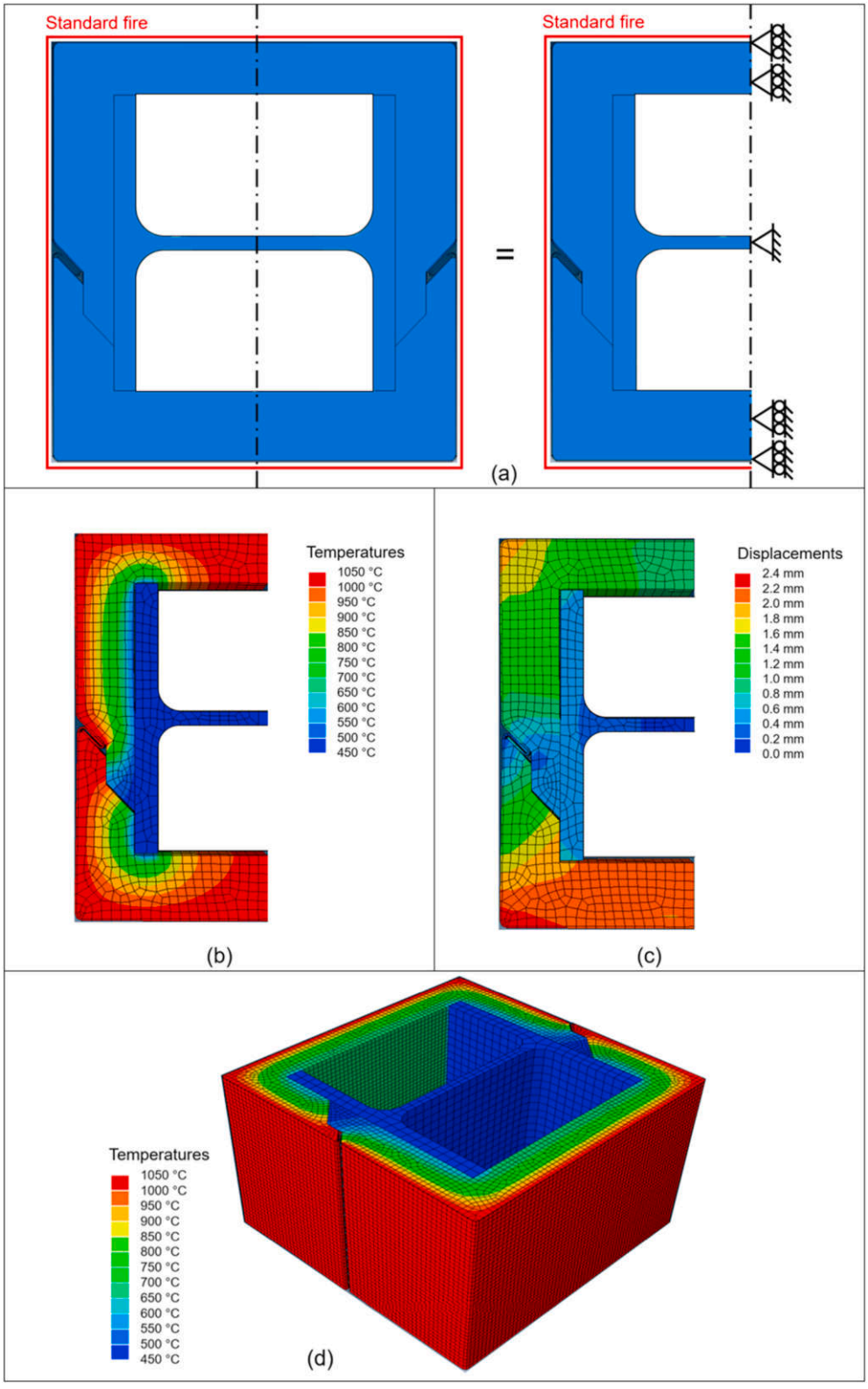

Fig. 11. Abaqus 3D numerical model: a) Numerical boundary conditions; b) Temperature field after 120 min of exposure to the standard fire; c) Displacement field after 120 min of exposure to the standard fire; d) 3D view of the temperature field after 120 min of exposure to the standard fire.

the experimental steel temperature achieved after 120 min of exposure to the standard fire curve. In greater detail, for Specimens 1, 2, 3, 5 and 7, TC values calibrated with Eq. (1) varied from −14% to +16.5% with respect to the theoretical value. Specimen 6 presented a TC value 77% higher than the theoretical one. The holes around the connection claws, constituting thermal bridges, should have been highlighted by the 2D numerical model. Although that was not the case, it is important to take that result into consideration to encompass the thermal effects of the holes. Specimen 4 exhibited a TC value 310% higher than the theoretical one. That important contrast with numerical predictions is assumed

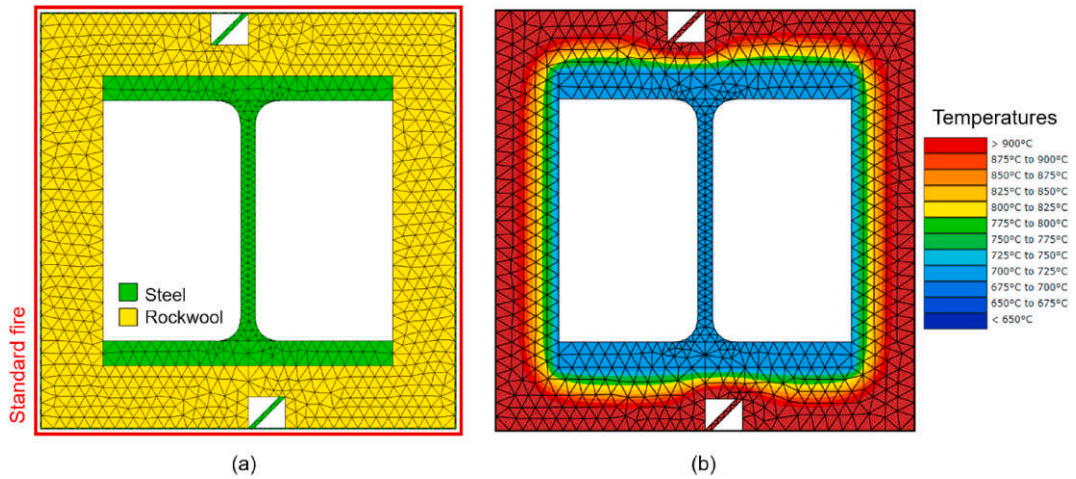

Fig. 12. 2D numerical model of Specimen 6: a) Cross-section discretisation with a mesh size of 6 mm; b) Temperature field within cross-section after 120 min of exposure to standard fire.

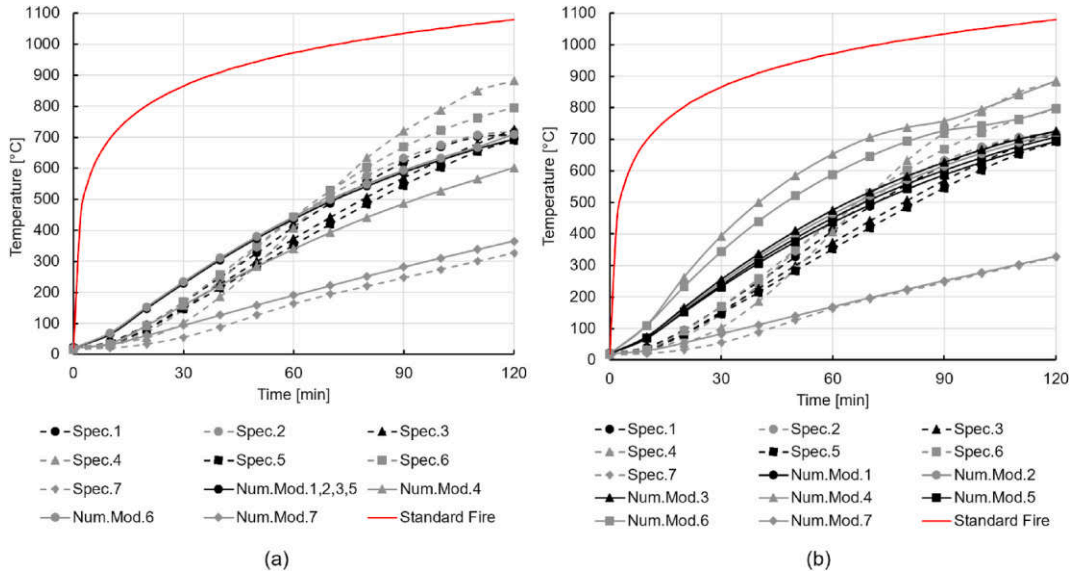

Fig. 13. Experimental- and numerical temperature evolutions with time using: a) theoretical TC value λ_{RW}; b) calibrated TC values $\lambda_{Num.i}$.

Table 4
List of coefficients and calibrated thermal conductivity values with 2D numerical models.

Specimen	Profile	Box section factor	Protection thickness	Theoretical thermal conductivity	Calibration coefficient	Calibrated thermal conductivity
		A_p/V [m^{-1}]	d_p [mm]	λ_{RW} [W/Km]	$c_{Num.i}$ [-]	$\lambda_{Num.i}$ [W/mK]
1	HEB140	134	30	0.20	1.060	0.212
2	HEB140	134	30	0.20	1.115	0.223
3	HEB140	134	30	0.20	1.165	0.233
4	HEB100	161	50	0.20	3.100	0.620
5	HEB140	134	30	0.20	1.000	0.200
6	HEB140	134	30	0.20	1.770	0.354
7	HEM220	64	45	0.20	0.860	0.172

coming from significant manufacturing defects. That result was therefore disregarded.

Based on TC values calibrated with 2D numerical models, the average value and standard deviation could be computed neglecting the value of Specimen 4, as expressed in Eq. (2) and Eq. (3) (where i is not assigned with the value 4). In guidelines for proper application of the standard of regulation EN1990 [32], it is recommended to define thermal characteristics by considering either the average value λ_{avg} or the 50th fractile of a beta distribution, $\lambda_{\beta,50\%}$. With average TC value λ_{avg} and standard deviation σ, it was possible to compute parameters α and β defining the beta distribution characterising TC values. The 50th fractile was computed from that beta distribution and expressed in Eq. (4).

$$\lambda_{avg} = \frac{\sum_{i=1}^{7} \lambda_{num,i}}{6} = 0.232 \quad [W/mK] \tag{2}$$

$$\sigma = \sqrt{\frac{\sum_{i=1}^{7}\left(\lambda_{num,i} - \lambda_{avg}\right)^2}{6}} = 0.058 \quad [W/mK] \tag{3}$$

$$\lambda_{\beta,50\%} = 0.229 \quad [W/mK] \tag{4}$$

It can be observed that the average TC value λ_{avg} and the 50th fractile obtained with the beta distribution $\lambda_{\beta,50\%}$ present very close values. Nevertheless, since λ_{avg} appeared slightly more conservative than $\lambda_{\beta,50\%}$, it was decided to consider the average TC value to predict the fire protection thermal efficiency. Therefore, Fig. 14a depicts temperature evolutions with time obtained with numerical models when applied with the average TC value. It has to be noted that only one curve was plotted for Specimens 1, 2, 3, 5 and 6 because the numerical models applied with λ_{avg} provided highly similar temperature evolutions with time, i.e. the difference of temperature were between 5 °C and 10 °C after 120 min.

For all the Specimens, it can be observed that numerical models provided temperature evolutions with time higher than the experimental ones when applied with λ_{avg}. However, for Specimen 6, that evolution was lower than experimental results between 75 and 120 min. In greater detail, differences of temperature between numerical predictions and experimental data are plotted in Fig. 14b for Specimens 1, 2, 3, 5, 6 and 7. It is possible to observe that higher numerical discrepancies, i.e. larger than 20%, occur at the beginning of the heating because the rock wool is characterised by a lower TC value at low temperatures than the one selected for calibration, which instead well represents the rock wool TC value after 120 min of exposure. In fact, after 75 min the difference is below 20%. Eventually, the development and calibration of 2D numerical models based on experimental results permitted the definition of an average TC values λ_{avg}. The use of this value facilitated reasonable predictions of the fire protection thermal efficiency when applied with the 2D numerical models.

4.3. Analytical model

This section uses the analytical model prescribed in EN1993-1-2 [25] to check its ability to predict the temperature evolution in the steel profile by assuming the calibrated value of the TC identified in the previous section. This analytical model calculates the temperature evolution with time of a protected steel profile based on a mass lumped approach. However, it is endowed with some limitations. As depicted in

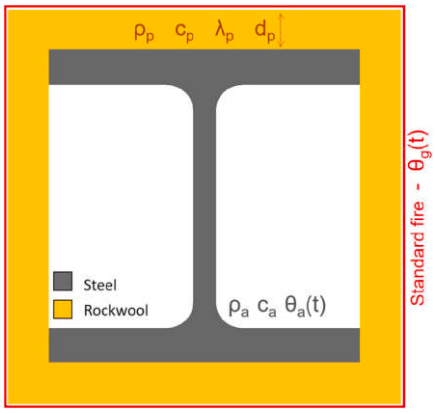

Fig. 15. Representation of the cross-section with the analytical model.

Fig. 15, the model only considers a single and uniform insulation layer. Therefore, specimens cannot be faithfully represented with the steel sheet surrounding the rock wool layer and the irregularities around connection levels. The analytical formula expressing the temperature evolution with time of a protected steel profile is defined in Eq. (5), where ϕ is the amount of heat stored in the protection as expressed in Eq. (6).

$$\Delta\theta_a(t) = \frac{\lambda_p A_p/V}{d_p c_a \rho_a}\cdot\frac{\left(\theta_g(t) - \theta_a(t)\right)}{\left(1+\frac{\phi}{3}\right)}\Delta t - \left(e^{\varphi/10} - 1\right)\Delta\theta_g(t) \quad [°C] \tag{5}$$

$$\varphi = \frac{c_p . d_p . \rho_p}{c_a . \rho_a}\cdot\frac{A_p}{V} \quad [-] \tag{6}$$

In the same manner as for numerical models, the evolution with time of the gas temperature $\theta_g(t)$ followed the standard fire curve, and thermal properties considered for steel and rock wool materials, are the ones from EN1993-1-2 and the ones listed in Table 3, respectively. Similarly to the observations made with 2D numerical models, Fig. 16a shows that the analytical model, when applied with theoretical values, provided lower temperature evolutions with time than experimental ones for Specimens 1, 2, 3, 4, 5 and 6, while the opposite was observed with Specimen 7. In greater detail, after 120 min, differences of temperature between analytical predictions and experimental tests equal to −6%,

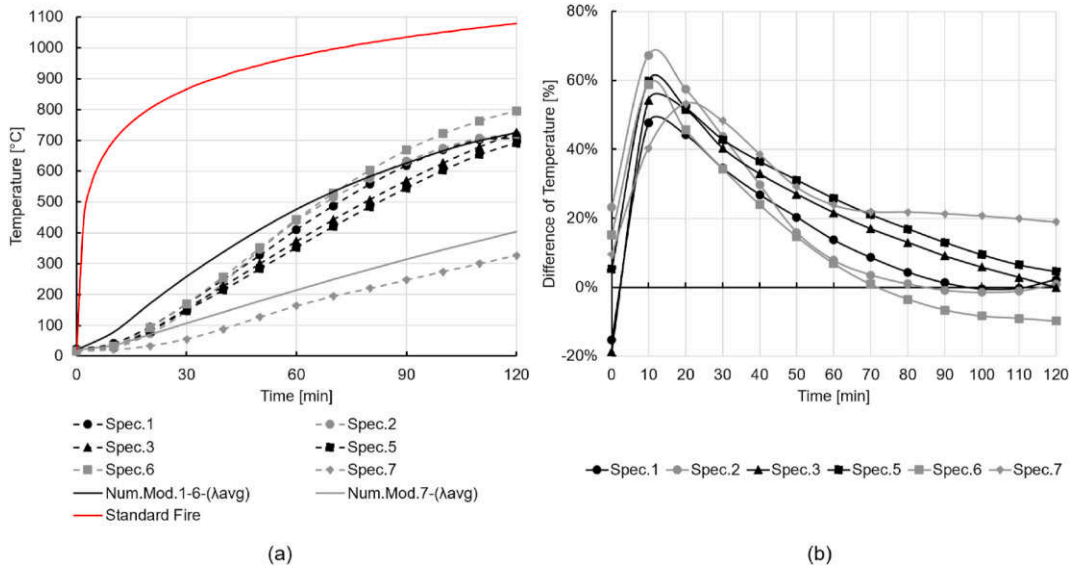

Fig. 14. a) Experimental- and numerical temperature evolutions with time using average TC value λ_{avg}; b) Differences between experimental- and numerical temperatures.

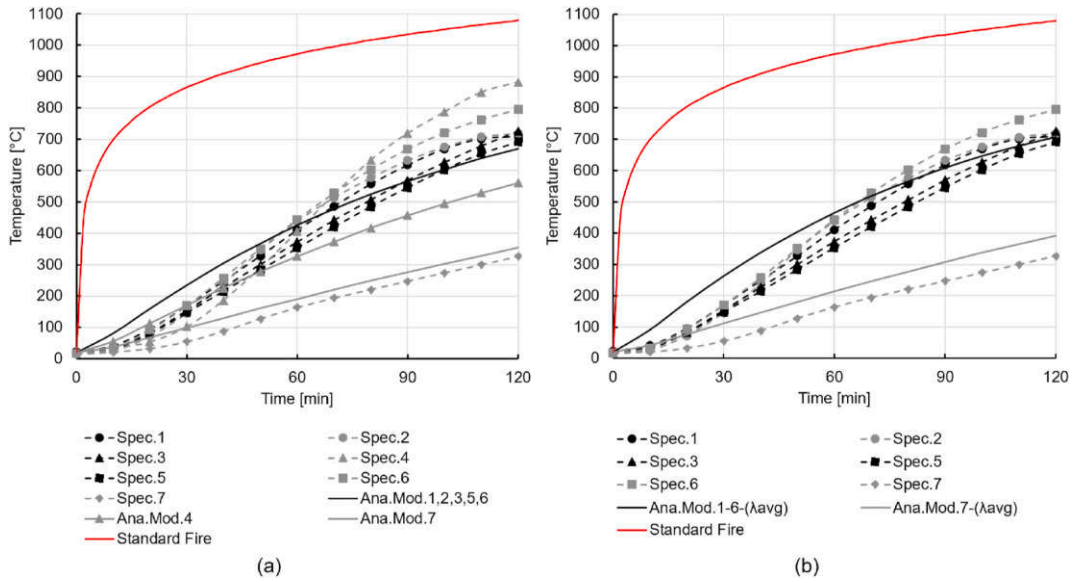

Fig. 16. Experimental- and analytical temperature evolutions with time using: a) theoretical TC value λ_{RW}; b) average TC values λ_{avg}.

−7%, −8%, −57%, −3%, −19% and +8% were respectively observed for Specimens 1, 2, 3, 4, 5, 6 and 7.

Fig. 16b depicts temperature evolutions with time obtained with the analytical model when applied with the average TC values λ_{avg} computed in the previous section. Results are similar to the ones observed with 2D numerical models. The analytical model provided a temperature evolution with time close from the experimental ones when applied with λ_{avg}, for Specimens 1, 2, 3, 5, whereas for Specimen 6, that evolution was lower than the experimental result after 70 min. For Specimen 7, the temperature evolution obtained with λ_{avg} was higher than experimental results. More specifically, after 120 min, differences of temperature between analytical predictions and experimental tests of −0.2%, −1.7%, −2.6%, +2.2%, −12% and +16.6% were respectively observed for Specimens 1, 2, 3, 5, 6 and 7.

Globally the analytical model allowed the assessment of the TC values calibrated with the 2D numerical model. It may be observed that both numerical and analytical models provided similar results. The average TC values λ_{avg} was therefore considered in Section 5 as indicator for the definition of the large-scale experimental campaign.

4.4. Predictions with the regression model

An alternative method to assess and predict the efficiency of a fire protection based on experimental test results can be found in Annex E.3 of the European standard of regulation EN13381-4 [26]. In this method, for a predefined steel design temperature θ_a, the TC value to be used with different protection geometries, is defined as a function of the thickness of the protection d_p [m] and the box section factor A_p/V [m^{-1}] of the protected profile. This function is obtained by linear regression, as expressed in Eq. (7).

$$\lambda_{\theta a}\left(A_p / V, d_p\right) = a_0 + a_1.A_p / V + a_2.d_p \quad [W / mK] \tag{7}$$

The coefficients a_0, a_1 and a_2 are found by applying the least squares method with the TC values determined with the analytical model based on experimental results. For design temperatures in the range of 350 °C–600 °C with step equal to 50 °C, coefficients a_0, a_1 and a_2 can be defined by using the data of all the Specimens except for Specimen 4. For each Specimen, considering the recorded times to reach design temperatures it was straightforward to determine the corresponding TC values using the analytical model with Eq. (5) depicted in section 4.3. For each Specimen, times to reach the different design temperatures and the corresponding TC values are summarized in Table 5 and Table 6, respectively. It has to be noted that for Specimen 7, the times to reach 550 °C and 600 °C were estimated based on experimental results by linear extrapolation. Subsequently, for each design temperature, coefficients a_0, a_1 and a_2 were defined by linear regression using the TC values corresponding to each specimen. Eventually, these coefficients are defined in Table 7 for each design temperature and computed with Eq. (7). In this respect, Fig. 17 illustrates the function $\lambda_{\theta a}(A_p/V, d_p)$ for a design temperature T_i equal to 600 °C.

Subsequently, function $\lambda_{\theta a}(A_p/V, d_p)$ could be used with the analytical model to evaluate the mean temperature of a protected profile after a time period t. Nevertheless, it must be ensured that the resulting temperature at time t is in accordance with the design temperature θ_a associated to the considered function $\lambda_{\theta a}$. Since a significant difference was observed between Specimens 1 2 3 5 6 and Specimen 7 presenting

Table 5
Times for specimens to reach design temperatures.

Time [min]									
Specimen	Profile	Box section factor Ap/V [m^{-1}]	Thickness d_p [mm]	Design temperatures θa [°C]					
				350	400	450	500	550	600
1	HEB140	134	30	53	59	65	72	79	87
2	HEB140	134	30	50	56	61	68	76	84
3	HEB140	134	30	57	64	71	79	87	95
5	HEB140	134	30	60	67	75	83	91	99
6	HEB140	134	30	50	55	61	67	73	80
7	HEM220	64	45	129	147	165	176	186[a]	195[a]

[a] Time extrapolated based on experimental results.

Table 6
TC values corresponding to specimens for each design temperature.

Thermal conductivity value [W/mK]									
Specimen	Profile	Box section factor A_p/V [m^{-1}]	Thickness d_p [mm]	Design temperatures θ_a [°C]					
				350	400	450	500	550	600
1	HEB140	134	30	0.173	0.185	0.199	0.210	0.223	0.236
2	HEB140	134	30	0.186	0.198	0.215	0.226	0.235	0.247
3	HEB140	134	30	0.158	0.168	0.179	0.187	0.197	0.211
5	HEB140	134	30	0.149	0.158	0.166	0.175	0.186	0.200
6	HEB140	134	30	0.186	0.203	0.215	0.230	0.247	0.264
7	HEM220	64	45	0.181	0.188	0.196	0.215	0.238[a]	0.265[a]

[a] TC value determined based on extrapolated time.

Table 7
Regression coefficients.

Regressions coefficient	Design temperatures θ_a [°C]					
	350	400	450	500	550	600
a_0	0.10374	0.10804	0.11233	0.12350	0.13566	0.14946
a_1	0.00016	0.00023	0.00029	0.00023	0.00017	0.00011
a_2	1.48399	1.45319	1.44913	1.70899	1.97515	2.25396

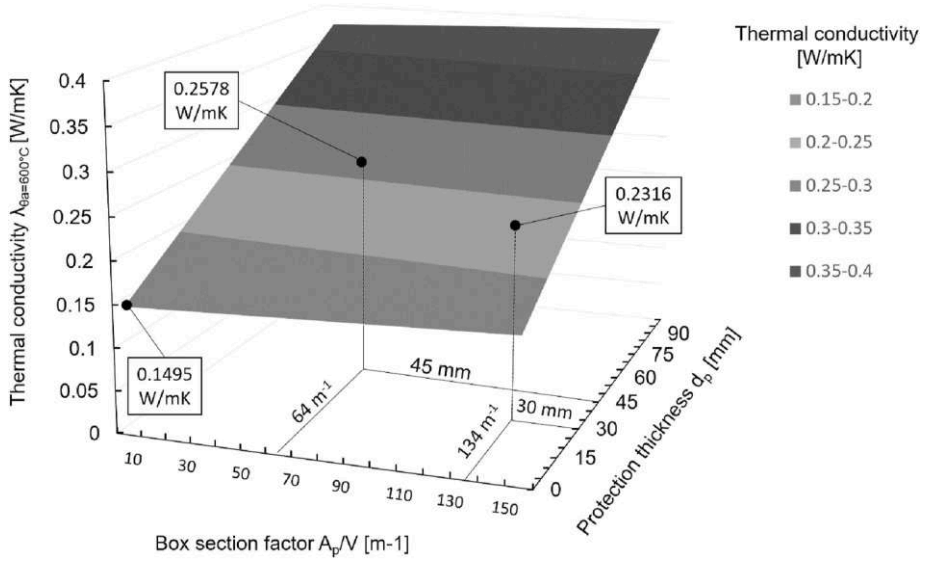

Fig. 17. Definition of $\lambda_{\theta a}$ (A_p/V,d_p) for a design temperature θ_a of 600 °C.

precisely different protection thicknesses and box section factors, this method appeared relevant to be applied here. Table 8 compares the TC values calibrated with the 2D numerical model and the ones predicted here with the regression model based on temperature values after 120 min of exposure to the standard fire curve. It appeared that the function $\lambda_{\theta a}(A_p/V, d_p)$ provided a TC value for Specimens 1 2 3 5 6 very close to the average TC value λ_{avg} (0.2316 W/mK against 0.2320 W/mK) and a more conservative TC value for Specimen 7. This function was also considered in Section 5 as indicator for the definition of the large-scale experimental campaign.

Table 8
Comparison between calibrated- and predicted TC values based on temperature values after 120 min of exposure to the standard fire curve.

Thermal conductivity value [W/mK]						
Specimen	Profile	Box section factor A_p/V [m^{-1}]	Thickness d_p [mm]	Calibrated TC values $\lambda_{Num.i}$ [W/mK]	Predicted TC values $\lambda_{\theta a}$ (A_p/v, d_p) [W/mK]	$\lambda_{\theta a}/\lambda_{Num.i}$
1	HEB140	134	30	0.212	0.2316	1.09
2	HEB140	134	30	0.223	0.2316	1.04
3	HEB140	134	30	0.233	0.2316	0.99
5	HEB140	134	30	0.200	0.2316	1.16
6	HEB140	134	30	0.354	0.2316	0.65
7	HEM220	64	45	0.172	0.1810	1.05

5. Large-scale experimental tests

5.1. Objectives

Small-scale experimental tests and calibrated models described in Section 3 and 4 aimed at assessing the potential of the fire protection. Since promising results were observed, it was decided to carry on the fire protection development by performing large-scale experimental fire tests. The execution of these large-scale tests had three objectives:

i) The first objective was to test other protection geometries and to collect additional data and to improve the understanding of the fire protection efficiency.
ii) The second objective was to study the thermo-mechanical behaviour of the protection in realistic conditions. For that purpose, the protection was installed around a steel column 3.1 m high and vertically loaded to 60% of its load bearing capacity. In such conditions, possible column flexural buckling characterised by out-of-plane displacements could affect the insulation efficiency of the protection by generating excessive stresses within the connection claws and consequently causing thermal bridges.
iii) The third objective of these large-scale experimental tests was to certify a final version of the fire protection, according to the European standard of regulation EN13381-4 [26]. This standard of regulation addresses passive fire protection systems preventing the heating of structural steel members (columns and beams) when exposed to standard fire, and it provides the experimental procedure to be adopted. For fires protection systems made of boards and addressing steel columns, the standard of regulation prescribes a "test package" to certify the protection when applied with *any thicknesses*, around *any profiles,* for *one fire resistance.* Nevertheless, this "test package" requires the successful experimental tests of 15 specimens, 2 loaded columns and 13 unloaded columns. Considering the stage of the protection development and the important costs of experimental tests, the scope of this large-scale experimental campaign was limited to the certification of one single version of the protection. The final version of the protection developed here, presents one insulation thickness and addresses a limited range of profiles, aiming at maintaining their temperature below 550 °C after 120 min of exposure to standard fire. In the framework of the present work, the number of specimens to test was therefore reduced to 5 specimens, 1 loaded column and 4 unloaded columns.

5.2. Final version of the fire protection system

Before the large-scale experimental tests and the subsequent assessment according to the European standard of regulation EN13381-4 [26] had to be selected. The features of the final protection version derived from small-scale experimental tests described in Section 3. They are listed here below and emerged based on observations made during the specimen manufacturing process and on considerations regarding installation ease and costs.

Absence of intumescent joint - Initially, it was planned to use intumescent joints at the connection level to ensure insulation in case of thermal bridge due to the thermal expansion of the protections. Eventually, it appeared unnecessary as described in Section 3.

Discontinuity of rock wool boards - Finally, instead of using intumescent joints at connection levels, proper discontinuity of rock wool boards at connection level was found to be a measure efficient enough to mitigate potential thermal bridges. Therefore, the total insulation layer thickness of the final protection version must be composed of two boards facilitating the creation of discontinuities at connection levels and within the corner as depicted in Fig. 2.

Discontinuity of male claws - Based on observations made with small-scale experimental tests, the discontinuity of male claws significantly made the protection installation easier without presenting any issues in terms of thermal and mechanical resistance.

Square holes around connection claws - It is the unwilling result from an optimized fabrication process. Since it is much more convenient to shape rock wool boards with rectangular sections, it was decided to fill the total thickness of the rock wool with the use of two boards. The exterior board presents a fixed thickness of 15 mm, which corresponds to the depth of the claw inside the protection. The thickness of the interior board is set to 30 mm. Consequently, the final version of the protection has a total rock wool thickness of 45 mm. However, in further developments of the fire protection, the thickness of the interior board could be affected by any value depending on the targeted fire resistance. The negative thermal impact of the hole at the connection level is mitigated by the rock wool board discontinuity.

Steel sheet thickness - The thickness of the steel sheet composing the protection structure was set to 0.7 mm. Preliminary tests demonstrated that using a thickness of 0.5 mm or 1 mm led for both cases to conclusive thermal results. However, during the prototype development, it appeared that 0.5 mm thick steel sheets were more subjected to plastic deformations in case of accidental blow. On the other hand, using 1 mm thick steel sheets led to excessive weight and undue costs. With these considerations, a thickness of 0.7 mm was selected as a compromise between the two tested thicknesses. Furthermore, it can be shown with numerical analyses that the use of thinner steel sheets (i.e. 0.5 mm) induces higher steel temperatures than the use of thicker ones (i.e. 1 mm). That is due to the fact that a thicker steel sheet can store more heat and consequently acts as a larger heat sink. Therefore, in this research work, it was decided to certify the fire protection system with a steel sheet thickness of 0.7 mm, which is more suitable for practical reasons.

Length of the connection claws - Different lengths of claws were tried with preliminary tests such as 6 mm, 8 mm and 12 mm. The objective was to facilitate the installation of the protection around a column by reducing the length of the claws. However, since the forces to be applied remained important, it was decided to the keep the original length of 12 mm to prevent claws disconnection in case of significant thermal expansion.

5.3. Specimens and instrumentation

Five specimens were tested in the fire laboratory at the University of Liège, Belgium. This laboratory is accredited to deliver European certifications based on experimental results. The furnace at the University of Liège allowed the simultaneous performance of the five experimental tests. The furnace presents a pentagonal basis 3.1-m high and the heating system is composed of gas burners. Among the five tests, one specimen was thermo-mechanically tested in the centre of the furnace while the four others were only thermally tested around the central column. The arrangement of the specimens within the furnace is depicted in Fig. 22.

The properties of the five specimens are defined in Table 9 and their geometries are depicted in Fig. 18 and Fig. 19. As defined in previous Section, the final version of the fire protection presents a rock wool thickness of 45 mm, composed of two boards of 15 mm and 30 mm and surrounded by a 0.7 mm thick steel sheet, and there are square holes around the connection claws. This geometry is identical to the one of Specimen 7 tested in the small-scale experimental campaign.

Before the test, the five specimens were arranged in the furnace with appropriate thermal boundary conditions. As illustrated in Fig. 20a, to make quasi-adiabatic boundary conditions at the top and bottom of the unloaded specimens, they were laid on 30 mm thick rockwool boards and 25 mm of ceramic fibre. The top of the specimens was covered with ceramic fibre and a rock wool board, on which a brick of cellular concrete was applied to minimise thermal bridges. Regarding the loaded specimen, the steel plates welded at its extremities for the proper load application, were wrapped with ceramic fibre to minimise heat transfer (Fig. 20b). Additionally, for the five specimens, 30 mm thick rock wool

Table 9
Properties of the large-scale experimental tests.

Specimen	Profile	Height [m]	Loaded/ Unloaded	Box section factor [m^{-1}]	Rock wool thickness [mm]	Steel sheet thickness [mm]	Discontinuity of the claws	Claws length [mm]	Identical half-protections	Hole at the connection level	Intumescent joint
8	HEB240	1.0	Unloaded	94	45	0.7	Yes	12	Yes	Yes	No
9	HEB320	1.0	Unloaded	80	45	0.7	Yes	12	Yes	Yes	No
10	HEM220	1.0	Unloaded	64	45	0.7	Yes	12	Yes	Yes	No
11	HEM400	1.0	Unloaded	46	45	0.7	Yes	12	Yes	Yes	No
12	HEM220	3.1	Loaded	64	45	0.7	Yes	12	Yes	Yes	No

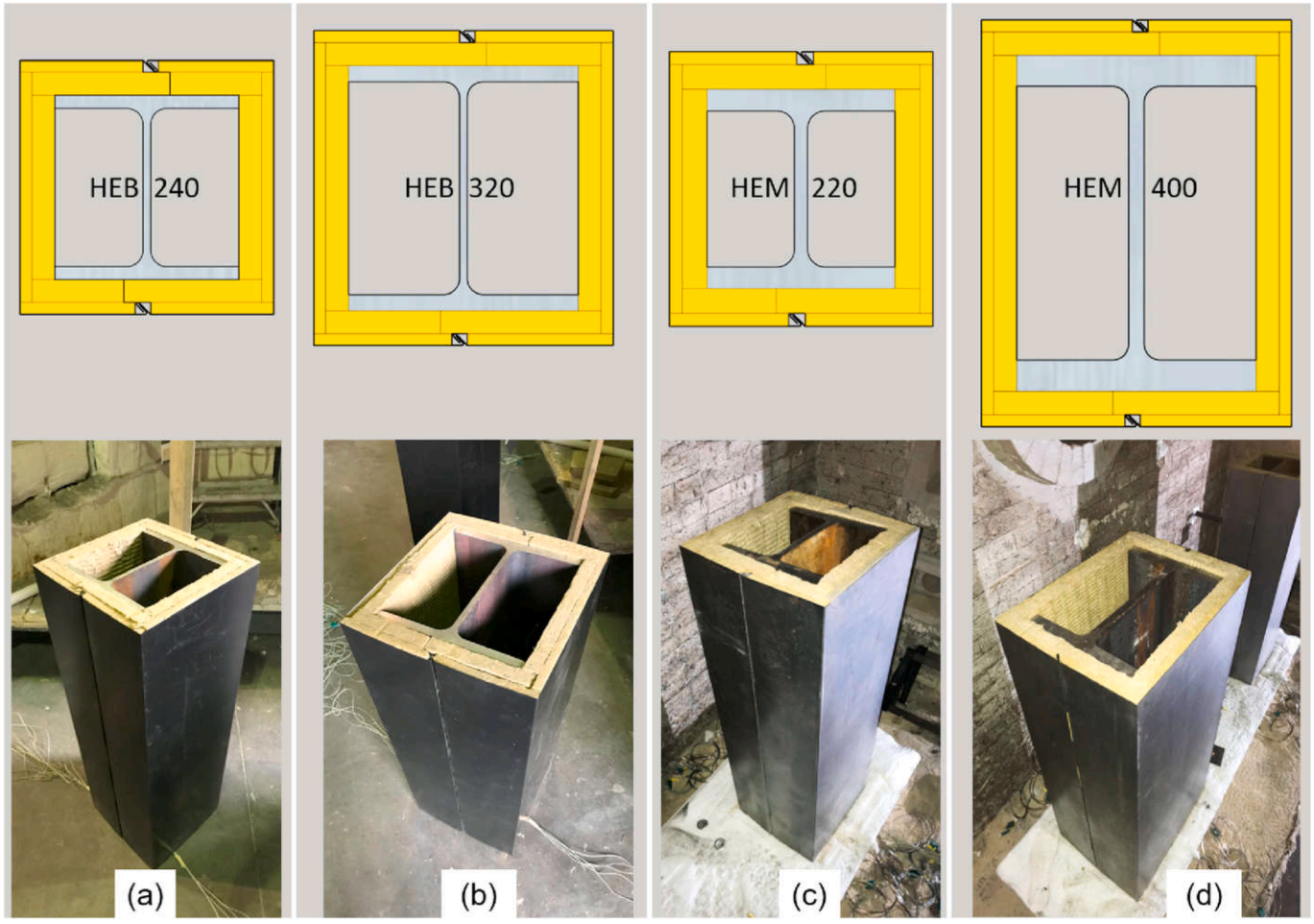

Fig. 18. Description of the unloaded specimens: a) Specimen 8; b) Specimen 9; c) Specimen 10; d) Specimen 11.

boards were inserted between the flanges at the top and bottom of the profiles (Fig. 20c). Each fire protection was properly installed around steel profiles. However, two claws were disconnected at the top of the loaded column and they remained too hard to connect, as illustrated in Fig. 20d. This was due to excessive thickness of rock wool resulting from manufacturing defect.

The protection was designed for columns of buildings requiring a fire resistance period of 120 min (R120), that can be found in several common occupancies, such as hotels, office buildings, schools, public buildings, etc. The analytical model depicted in Section 4.3 was used with the values of thermal conductivity calibrated in Section 4.2 and 4.4, i.e. λ_{avg} and $\lambda_{\theta a}$ (A_p/V,d_p), to predict the temperature of steel profiles characterised by different box section factors after 120 min of exposure to the standard fire, when equipped with a protection thickness of 45 mm. These temperature predictions are plotted in Fig. 21, as a function of the box section factor of the protected profile. Temperature values were calculated for box section factors A_p/V going from 30 m^{-1} to 150 m^{-1} with a step of 5 m^{-1}.

Considering the type of columns which usually requires a R120 fire protection, the range of profiles addressed by the final version of the protection was limited to box section factor values in the range of 46 m^{-1} and 94 m^{-1}, that represents HE steel profiles of section from HEM400 to a HEB240, respectively. The temperature of an HEB240 equipped with the protection after 120 min of exposure to standard fire, was estimated to 493 °C and 480 °C with the use of λ_{avg} and $\lambda_{500°C}$(A_p/V, d_p), respectively. These temperatures were more than 10% below 550 °C which constituted a margin for unforeseen thermal results in large-scale tests. HEB240 steel profile was therefore selected as the upper limit in term of box section factor. Additionally, it is not relevant to protect steel profiles for which the ratio between the protection thickness and the profile depth presents too high values. Based on these predictions, HEB240, HEB320, HEM220 and HEM400 S355 steel profiles were

Fig. 19. Description of the loaded specimen 12: a) unprotected; b) Protected.

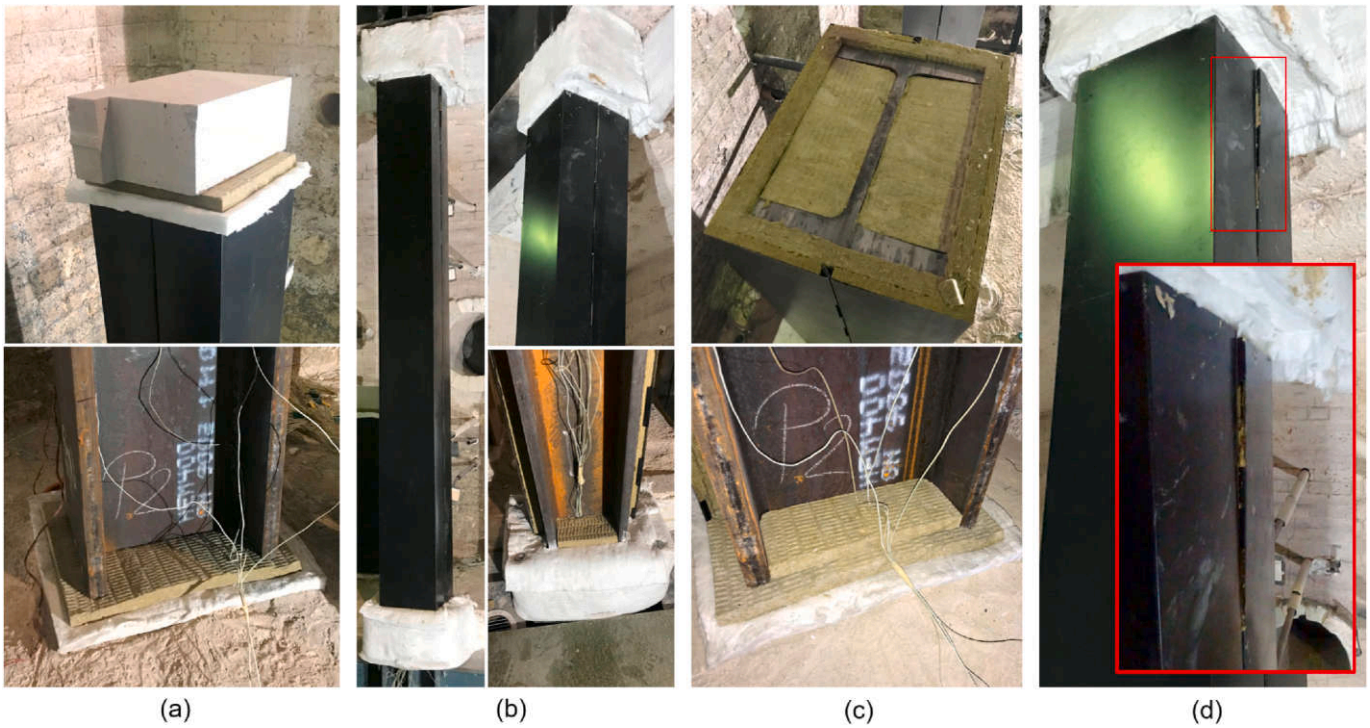

Fig. 20. Details of specimens: a) Boundary conditions of unloaded specimens; b) Boundary conditions of the loaded specimen; c) Rock wool boards between steel profile flanges; d) Disconnection of two claws.

selected to be the unloaded specimens. According to the standard of regulation, the loaded steel profile must be selected among the unloaded ones. That allows thermal efficiency comparison of two identical protections, when applied to loaded and unloaded columns. This comparison is detailed in Section 6.1. Furthermore, the loaded profile cannot be the one presenting the minimum or the maximum section factor. Therefore, an HEM220 S355 steel profile 3.1 m high was selected to be the loaded specimen.

The standard of regulation requires the concentric application of a vertical point load equivalent to 60% of the load bearing capacity of the column which corresponds to a load of 2505 kN in accordance with EN 1993-1-1 [33]. Two 50-mm thick steel plates were welded at the column extremities to distribute the load on the entire cross-section area. The loaded specimen was installed at the centre of the furnace within a steel frame controlled by two actuators. Boundary conditions of the loaded specimen were pinned-pinned about the weak axis and fixed-fixed about the strong axis, as required by the standard of regulation.

The arrangement of the specimens is illustrated with a plan view in

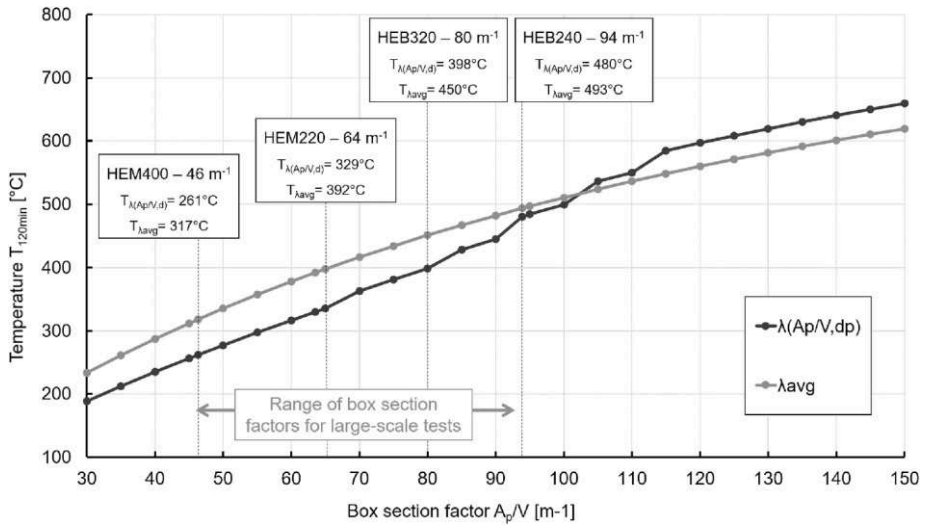

Fig. 21. Temperature predictions for profiles protected with 45 mm after 120 min of exposure to standard fire.

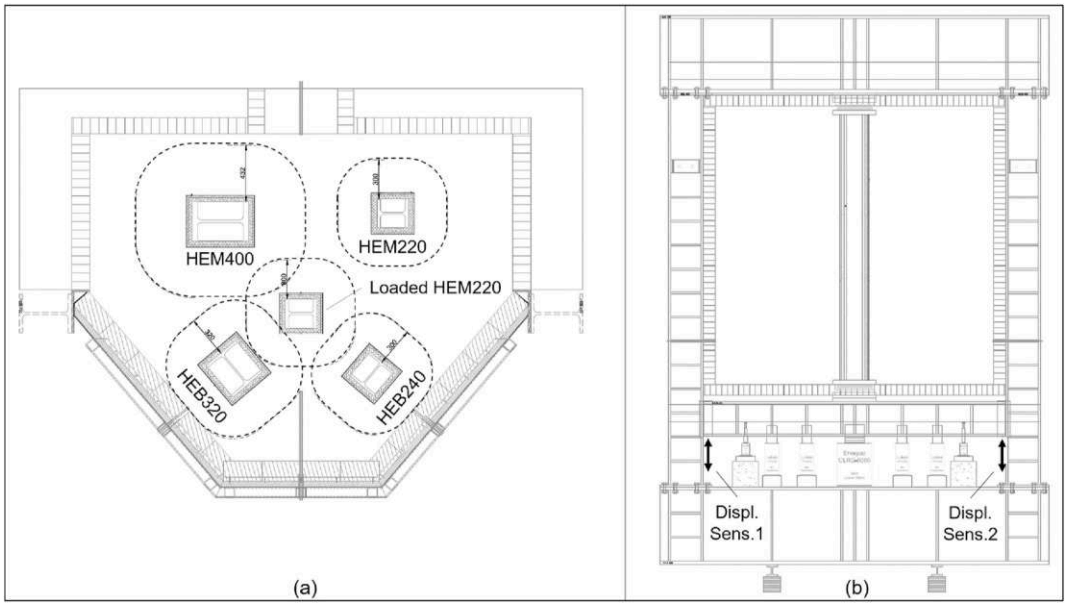

Fig. 22. Large-scale experimental furnace: a) plan view; b) transversal view.

Fig. 22a and respected the distance of separation prescribed by the standard of regulation as the maximum value between 300 mm and the depth of the protected profile. The steel frame loading Specimen 12 is illustrated in Fig. 22b, with the two displacement sensors located at the extremities of the beam applying the load. The four unloaded specimens were identically instrumented with 9 thermocouples. As depicted in Figs. 23a and 4 thermocouples were located at 500 mm from the bottom and 5 positioned at 800 mm. The loaded specimen was instrumented with 15 thermocouples. As depicted in Figs. 23b and 5 thermocouples were located at 1033 mm, 2067 mm and 2900 mm from the bottom.

5.4. Experimental uncertainties

The experimental results are characterised by uncertainty due to imperfections, instrumentation tolerances etc. Herein the main sources of uncertainty for the large-scale experimental tests are described. For instance, the readings obtained from the K-type thermocouples are typically affected by an error in the order of 1°C–2°C. In fact, the cables used at the University of Liège are of tolerance class 1, as defined in IEC 584-2 or equivalently in EN 60584-T2, and the tolerance values are: ±1.5 °C from −40 °C to 375 °C and ±0.004T from 375 °C to 1000 °C, i.e. max ±4 °C at 1000 °C. Moreover, the applied load can vary ±2% relatively to the nominal value. The gas temperature inside the furnace may be affected by deviation from the standard ISO 834 heating curve. In this respect, EN1363-1 [34] provisions give tolerances. In the first 5 min, no tolerance is prescribed because it is known that it is very difficult to precisely follow the curve in the first minutes of an experimental test owing to the quick change in the prescribed temperature. In Fig. 24 the evolutions as a function of time of the deviation and the tolerance of the full-scale test are shown. During the test the deviation is always below the maximum prescribed tolerance.

5.5. Experimental observations and results

Overall mean steel temperature evolutions with time resulting from the five specimens are depicted in Fig. 25. These temperatures result from the sum of the mean temperatures recorded at each level of thermocouples divided by the number of levels. For each specimen, mean

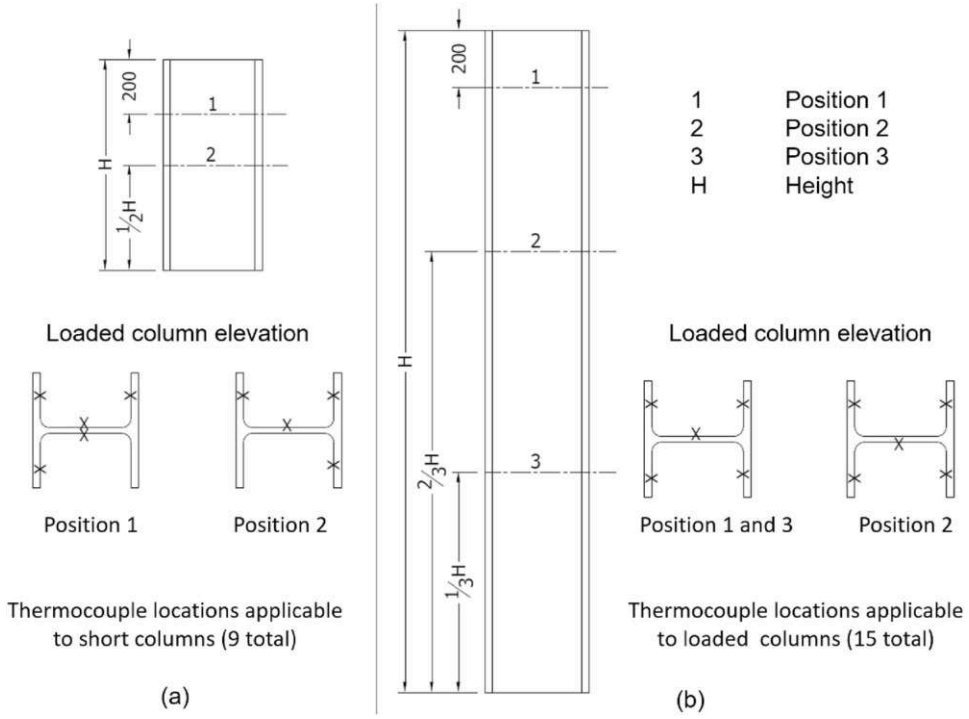

Fig. 23. Thermocouples locations issued by the standard of regulation EN13381-4: a) Unloaded specimens; b) Loaded specimen.

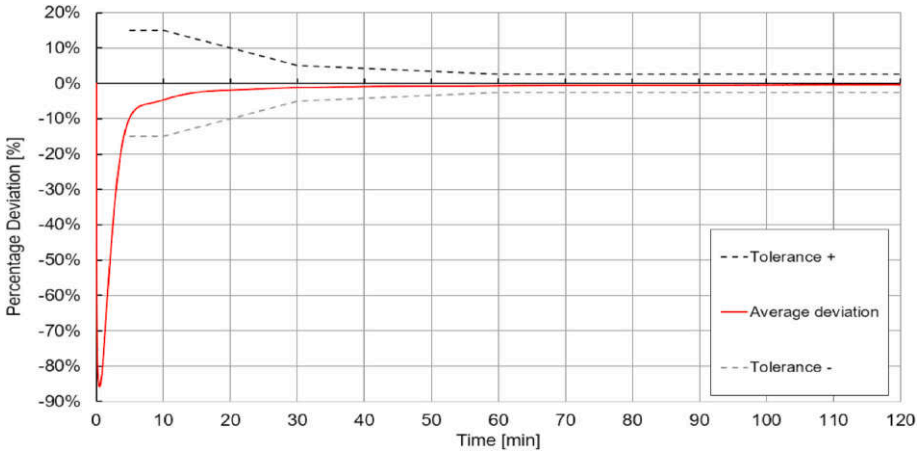

Fig. 24. Percentage deviation of the average temperature measured in the furnace.

temperatures recorded at each level of thermocouples are plotted in Fig. 26 to highlight thermal gradients within the specimens.

Regarding unloaded profiles, i.e. Specimens 8, 9, 10 and 11, they exhibited temperature evolutions with time that were higher for profiles with higher section factors. For each of them, it could be noticed that thermocouples located at 800 mm from the bottom, recorded slightly higher temperatures (+/- 13 °C) than thermocouples located at 500 mm. Overall mean temperatures recorded after 120 min of exposure to standard fire, for Specimens 8, 9, 10 and 11, were 398 °C, 358 °C, 334 °C and 245 °C, respectively. These thermal results are significantly better than predictions based on calibrated models built on the small-scale test results, as depicted Fig. 21, where these temperatures after 120 min were predicted to be 493 °C, 450 °C, 392 °C, 317 °C, respectively. That represents temperature differences between 15% and 25%. Furthermore, for the four specimens, after 120 min of exposure to the standard fire it was observed that protections were intact, and their connection claws remained closed as exposed in Fig. 28.

Regarding the loaded profile, i.e. Specimen 12, it exhibited different temperature-time evolutions at the three levels of thermocouples. In fact, thermocouples located at 2900 mm recorded significantly higher temperature evolutions with time than the ones located at 2067 mm and 1033 mm. This was due to the two claws which remained open. After 120 min of exposure to standard fire, mean temperatures recorded at 2900 mm, 2067 mm and 1033 mm were respectively 538 °C, 394 °C and 343 °C, generating an overall mean temperature of 425 °C. This temperature was 27.3% higher than the one observed with the unloaded Specimen 10 having the same geometry and 8% higher than the predicted temperatures of Fig. 21.

Mechanically, the load of 2505 kN was progressively applied on Specimen 12 in 15 min and was maintained then for 20 min before the furnace was switched on. The evolution with time of the axial displacement of the column is plotted in Fig. 27 and defined in equation Eq. (8) as the sum of the thermal expansion, expressed in Eq. (9) and the mechanical one. As illustrated on the graph, the thermal expansion is considered positive since it tends to increase the height of the profile while the axial displacement owing to mechanical loading is considered

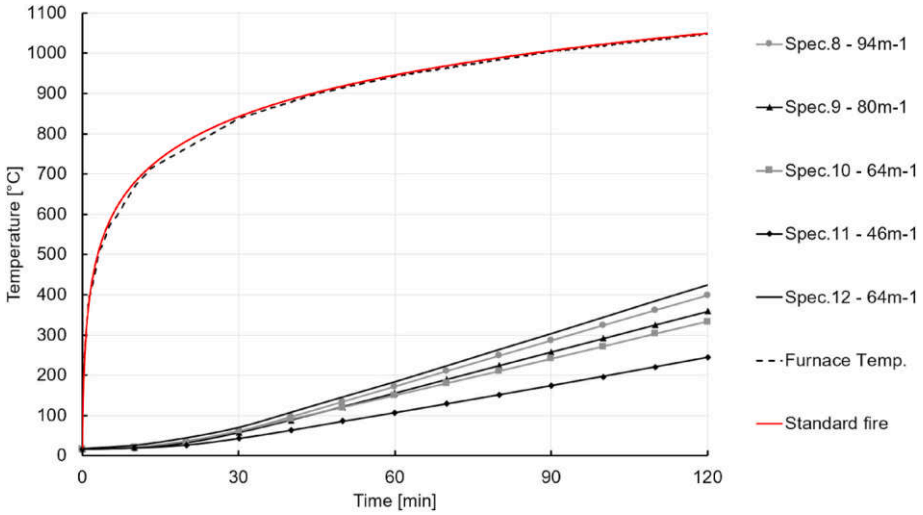

Fig. 25. Large-scale experimental tests results – Overall average temperature evolutions with time of the specimens characterised by different box section factor reported in the legend.

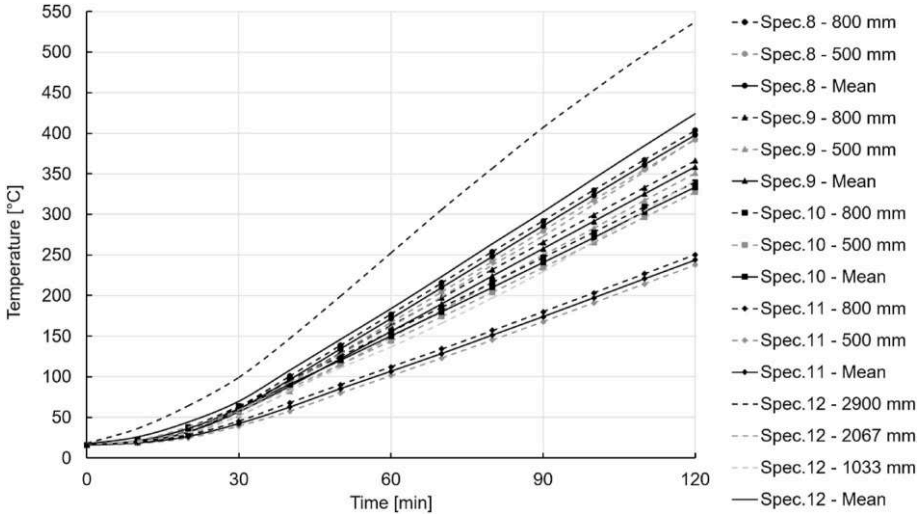

Fig. 26. Large-scale experimental tests results – Mean temperature evolutions with time at each location of thermocouples.

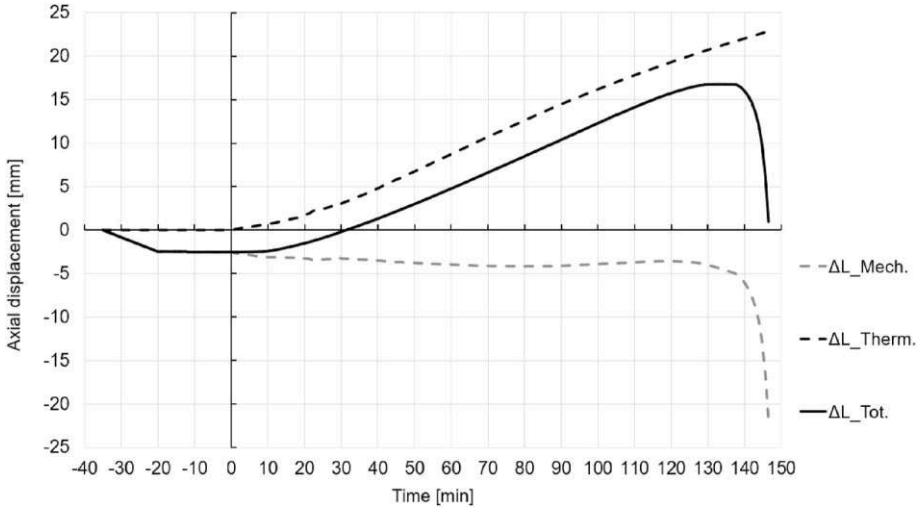

Fig. 27. Large-scale experimental tests results – Axial displacement evolution with time.

Fig. 28. Unloaded specimens after the 120 min of exposure to standard fire: a) Specimen 8; b) Specimen 9; c) Specimen 10; d) Specimen 11.

negative.

$$\Delta L_{Tot}(t) = \Delta L_{Therm.}(t) + \Delta L_{Mech.}(t) \quad [mm] \tag{8}$$

$$\Delta L_{Therm.}(t) = \Delta T(t).\alpha.L \quad [mm] \tag{9}$$

With

$$\Delta T(t) \quad = \quad T(t)\text{-}T_0 \quad [^{\circ}C] \tag{10}$$

In these equations, T(t) is the overall mean temperature of the loaded profile at the time t, T_0 is the overall mean temperature of the loaded profile at the beginning of the test, equal to 17 °C. α is the thermal expansion coefficient of steel, equal to 1.2 x 10^{-5} °C^{-1}. L is the height of the loaded profile, equal to 3.1 m.

After loading the column attained an axial displacement of −2.48 mm. After 10 min of exposure to standard fire, the column started to axially displace with constant rate of +0.15 mm/min. This displacement

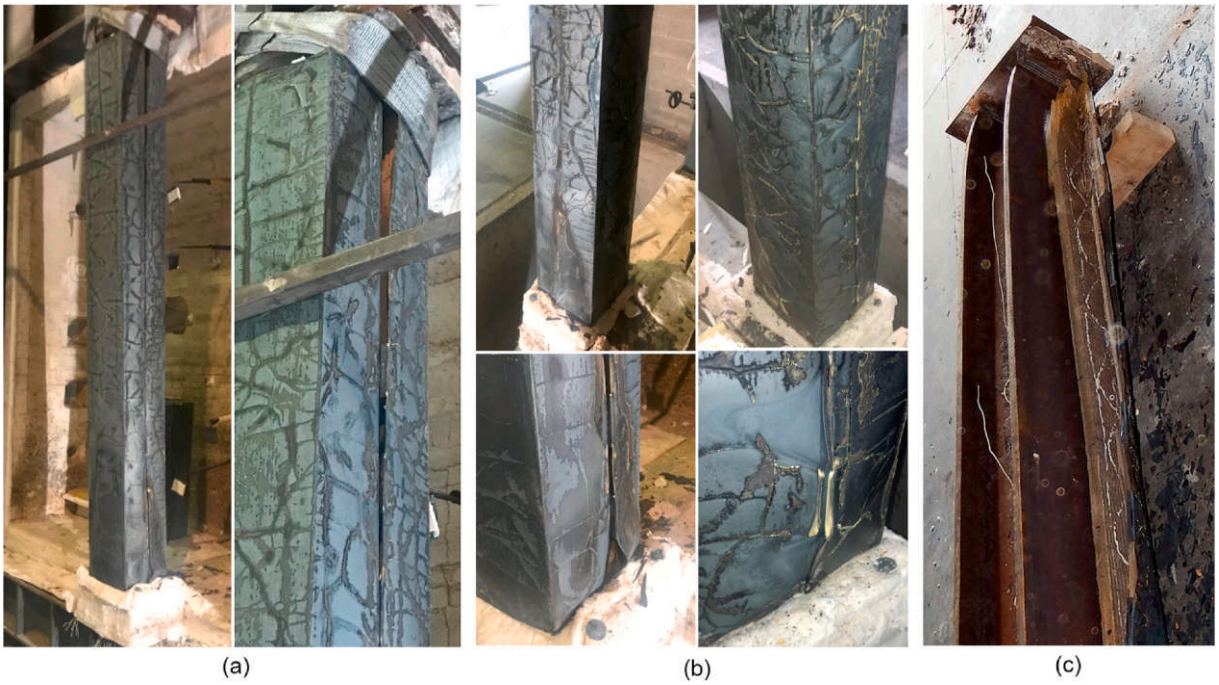

Fig. 29. Loaded specimen 12 after the 120 min of exposure to standard fire: a) Opening of two claws; b) Buckling of the steel sheets; c) Buckling of the HEM220 profile.

rate was due to thermal expansion of the column and occurred between 10 min and 130 min, which entailed a total axial displacement of +19 mm. Only after 138 min of exposure to standard fire, the column started to buckle at the top level of the specimen, where the average temperature of the column was 604 °C after 140 min, as illustrated in Fig. 29c. In fact, between 138 min and 146 min, a sudden column shortening was observed and at 146 min the load application was removed.

Besides the two claws disconnected during the experiment, all the other claws of the protection remained closed around the column during the test duration. As illustrated in Fig. 29, after the experiment, the protection was open at the top with a gap of +/- 4 cm (Fig. 29a), wider than at the beginning of the test namely due to the buckling of the profile (Fig. 29c). Moreover, the steel plates composing the protection were buckled at the bottom of the specimen (Fig. 29b). This was due to the thermal dilatation prevented by the end plates and due to the weight of the protection.

6. Assessment of the fire protection

6.1. Temperature data

This section aims at assessing the fire protection thermal efficiency according to the standard of regulation EN13381-4 [26]. In this way, the protection can be certified. For that purpose, the first step was to collect the experimental data resulting from the large-scale tests. Table 10 summarises the times for the different specimens to reach the design temperatures. Temperatures considered in this table are the overall mean temperatures calculated in Section 5.4. The standard of regulation evaluates the efficiency of the protection by individually considering every design temperature included in the scope of the assessment with step equal to 50 °C and starting from 350 °C.

Based on the times collected here above, the stickability performance of the protection is evaluated by comparing the results of Specimens 10 and 12. Correction factors k are calculated for each design temperature with the expressions defined in Eq. (11) and Eq. (12).

$$k = t_l / t_c \quad [-] \tag{11}$$

where

$$t_c = t_l . \frac{S_l}{S} . \frac{D}{D_l} \quad [\text{min}] \tag{12}$$

In these equations, k is the correction factor. t_l and t_1 are the times to reach a design temperature for the loaded and unloaded specimens, respectively. t_c is the corrected time for the unloaded specimen to reach the design temperature. S and S_1 are box section factors of the loaded and unloaded profiles. D and D_1 are protection thicknesses of the loaded and unloaded specimens. In the case of the present work, the protections of Specimens 10 and 12 are perfectly identical so that S equals S1 and D equals D1. The corrected time is therefore taken as the time for the unloaded specimen to reach the design temperature. Resulting correction factors k are calculated in Table 11. It has to be noted that correction factors for design temperatures of 550 °C and 600 °C are found by linear extrapolation based on correction factors calculated for 450 °C and 500 °C. Times for unloaded specimens to reach design temperatures are corrected against the loaded section and multiplied by the corresponding correction factor. Finally, the corrected time to be considered in the assessment procedure are summarized in Table 12.

6.2. Assessment procedure

To assess the performance of the fire protection system, Annex E of EN 13381-4 prescribes four methods leading to similar results. However, it is up to the protection developers to select the most appropriate method yielding the best relation between experimental data and protection performance. Based on the corrected times summarized in Table 12, all four methods were employed. In particular, the one described in Annex E.4 of the EN 13381-4 and referred to as the numerical regression analysis appeared to provide the best results. Therefore, only this method is developed here. The aim of that method is to predict the time t for a protected specimen to reach a design temperature θ_a, as a function of protection thickness d_p, box section factor A_p/V and design temperature θ_a, based on experimental results. That function is defined in Eq. (13) where parameters a_i are coefficients to be determined by solving the regression equation using all the corrected time summarized in Table 12. Since the fire protection thickness d_p is unique and equal to 45 mm in the framework of this certifying large-scale test, Eq. (13) can be simplified with Eq. (14) and written with a matrixial form in Eq. (15). Based on the 17 data summarized in Table 12, Eq. (15) can be expressed in its complete from.

$$t = a_0 + a_1 . b_p + a_2 . \frac{d_p}{A_p/V} + a_3 . \theta_a + a_4 . d_p . \theta_a + a_5 . d_p . \frac{\theta_a}{A_p/V} + a_6 . \frac{\theta_a}{A_p/V} + a_7 . \frac{1}{A_p/V} \quad [\text{min}] \tag{13}$$

$$t = b_0 + b1 . \frac{1}{A_p/V} + b_2 . \theta_a + b_3 . \frac{\theta_a}{A_p/V} \quad [\text{min}] \tag{14}$$

$$\underline{\underline{A}} . \underline{b} = \underline{t} \tag{15}$$

$$\begin{bmatrix} 1 & 1/94 & 350 & 350/94 \\ 1 & 1/94 & 400 & 400/94 \\ 1 & 1/94 & 450 & 450/94 \\ 1 & 1/94 & 500 & 500/94 \\ 1 & 1/94 & 550 & 550/94 \\ 1 & 1/94 & 600 & 600/94 \\ 1 & 1/80 & 350 & 350/80 \\ 1 & 1/80 & 400 & 400/80 \\ 1 & 1/80 & 450 & 450/80 \\ 1 & 1/80 & 500 & 500/80 \\ 1 & 1/80 & 550 & 550/80 \\ 1 & 1/64 & 350 & 350/64 \\ 1 & 1/64 & 400 & 400/64 \\ 1 & 1/64 & 450 & 450/64 \\ 1 & 1/64 & 500 & 500/64 \\ 1 & 1/46 & 350 & 350/46 \\ 1 & 1/64 & 400 & 400/46 \end{bmatrix} \cdot \begin{bmatrix} b_0 \\ b_1 \\ b_2 \\ b_3 \end{bmatrix} = \begin{bmatrix} 86.6 \\ 96.5 \\ 107.0 \\ 118.0 \\ 129.5 \\ 141.5 \\ 95.1 \\ 106.2 \\ 117.7 \\ 129.8 \\ 142.3 \\ 101.5 \\ 113.9 \\ 126.6 \\ 139.7 \\ 134.5 \\ 150.7 \end{bmatrix}$$

This matrix system is solved with the least squares method according to Eq. (16) and provides the values of coefficients b_i to be used with Eq. (14). Times to reach design temperatures can be predicted for every specimen and they are summarized in Table 13.

Table 10
Experimental times [min] to reach design temperatures.

Specimen	Profile	Box section factor	Design temperatures θ_a [°C]					
		A_p/V [m^{-1}]	350	400	450	500	550	600
8	HEB240	94	107.0	120.6	134.7	149.6	165.2	181.6
9	HEB320	80	117.4	132.6	148.3	164.5	181.5	–
10	HEM220	64	125.4	142.2	159.4	177.0	–	–
11	HEM400	46	166.2	188.2	–	–	–	–
12	HEM220	64	101.5	113.9	126.6	139.7	–	–

Table 11
Correction factors k.

Design temperatures θ_a [°C]					
350	400	450	500	550	600
0.810	0.801	0.794	0.789	0.784	0.779

Table 12
Corrected times [min] to reach design temperatures.

Specimen	Profile	Box section factor	Design temperatures θ_a [°C]					
		A_p/V [m^{-1}]	350	400	450	500	550	600
8	HEB240	94	86.6	96.5	107.0	118.0	129.5	141.5
9	HEB320	80	95.1	106.2	117.7	129.8	142.3	–
10	HEM220	64	101.5	113.9	126.6	139.7	–	–
11	HEM400	46	134.5	150.7	–	–	–	–

$$\underline{b} = \left(\underline{\underline{A}}^T \underline{\underline{A}}\right)^{-1} \underline{\underline{A}}^T \underline{t} \tag{16}$$

$$\underline{b} = \begin{bmatrix} -42.30 \\ 4328 \\ 0.230 \\ 0.460 \end{bmatrix}$$

These predicted times must fulfil the acceptability criteria required by the standard of regulation to ensure safe applications of the protection. These criteria are listed in Table 14. With the values of the coefficients b_i calculated based on corrected times with Eq. (16), it appeared that predicted times do not meet criteria 2 and 3. Provided that criteria 1, 2 and 3 are not met, the standard of regulation recommends the reduction of the regression coefficients b_i by multiplying them with a linear modification factor x. In the present case, the optimal modification factor was determined, as being equal to 0.97, and was applied to coefficients b_i, as defined in Eq. (17). The modified coefficients b_i' were subsequently used with Eq. (14) to recalculate the predicted times to reach design temperatures, which are summarized in Table 15.

$$\underline{b}' = x.\underline{b} \tag{17}$$

$$\underline{b}' = \begin{bmatrix} -40.98 \\ 4195 \\ 0.220 \\ 0.440 \end{bmatrix}$$

With the modified regression coefficients b_i', Eq. (14) can be transformed in Eq. (18) to yield the maximum box section factor of the protected profile, depending on the design temperature and the requested fire resistance time. Box section factors are summarized in Table 16 for different design temperatures and for different fire resistance times. This table presents the results of this assessment procedure, in a straightforward way for applications.

$$\frac{A_p}{V} = \frac{b_1' + b_3'\theta_a}{t - b_0' - b_2'\theta_a} \quad \left[m^{-1}\right] \tag{18}$$

6.3. Discussion of the results

Results from the large-scale experimental tests and the assessment procedure, both performed according to the standard of regulation 13381-4, led to define the applicability range of the fire protection system. The fire protection, defined in Sections 2 and 5.2 with a rock wool thickness of 45 mm and 0.7 mm thick steel sheets, can be used to protect steel members characterised by box section factors ranging from 46 m^{-1} to 94 m^{-1}. Since Specimen 12 carried 100% of the required load for a longer period than the test duration of 120 min, assessment results are consequently applicable for any fire resistance period, equal or inferior to 120 min. Furthermore, according to the standard of regulation 13381-4, the range of steel profiles addressed by the protection can be enlarged by 10% in terms of box section factors, leading to a range from 42 m^{-1} to 103 m^{-1}. Even though the fire protection system was assessed for steel members presenting 'I' and 'H' cross-sections, the system developed can also be applied with structural hollow cross-sections with the same range of box section factors.

7. Cost analysis

As mentioned in the introduction, costs relative to a fire protection system must be divided into two parts, direct- and indirect costs. This last section establishes an accurate estimation of the plug-and-play system direct cost and compare it with others fire protection systems, i.e. intumescent paints, sprays and boards. Direct costs were straightforward to evaluate by considering actual prices of the specimens manufactured for experimental campaigns and the time spent for their production and installation. Indirect costs were far less straightforward to estimate due to the lack of data. For this reason, indirect costs were not quantified but only discussed.

Table 14
Acceptability criteria issued by the standard of regulation EN13381-4 [26].

1	For each specimen, the predicted time shall not exceed the corrected time by more than 15%
2	The mean value of all percentage differences as calculated in 1 shall be less than zero
3	A maximum of 30% of individual values of all percentage differences as calculated in 1 shall be more than zero
4	As the section factor increases the fire resistance time decreases, provided all other parameters remain constant
5	As the fire resistance time increases the temperatures increases, provided all other parameters remain constant
6	As the section factor increases the temperatures increases, provided all other parameters remain constant

Table 13
Predicted times [min] to reach design temperatures.

Specimen	Profile	Box section factor	Design temperatures θ_a [°C]					
		A_p/V [m^{-1}]	350	400	450	500	550	600
8	HEB240	94	84.6	96.1	107.7	119.2	130.8	142.3
9	HEB320	80	93.0	104.5	116.1	127.7	139.3	–
10	HEM220	64	107.4	119.1	130.8	142.4	–	–
11	HEM400	46	133.8	145.6	–	–	–	–

Table 15
Final predicted times to reach design temperatures.

Specimen	Profile	Box section factor	Design temperatures θ_a [°C]					
		A_p/V [m^{-1}]	350	400	450	500	550	600
8	HEB240	94	82.0	93.2	104.4	115.6	126.8	138.0
9	HEB320	80	90.1	101.3	112.6	123.8	135.0	–
10	HEM220	64	104.2	115.5	126.8	138.1	–	–
11	HEM400	46	129.7	141.2	–	–	–	–

Table 16
Maximum box section factors Ap/V [m^{-1}].

Time [min]	Design temperatures θ_a [°C]					
	350	400	450	500	550	600
60	177.8[a]	323.2[a]	–	–	–	–
90	79.9	100.5[a]	134.8[a]	203.9[a]	–	–
120	51.5	59.5	70.2	85.5	108.9[a]	149.7[a]

[a] Box section factors not tested experimentally.

Direct cost is detailed in Table 17 as the sum of the material and labour costs. Data for the material cost estimation were taken from the suppliers [28,34,35]. Data for the labour cost estimation were based on observations and the European average hourly labour cost [36]. Direct cost is expressed as a unit cost [€/m^2] to be compared with other systems. Unit costs data for different fire protection systems are provided by the Bauforumstahl [37], i.e. a steel construction forum established in Dusseldorf, Germany. For each system, Table 18 defines unit cost ranges found for fire resistances of 30 min, 60 min, 90 min and 120 min. Unit cost for intumescent paints depends on the application method. It tends to be more expensive when applied on site than when pre-applied in the workshop. Unit costs for sprays and boards varies with the composition and the quality of the product. It must be noted that unit cost ranges for R120 fire resistance were estimated by linear extrapolation based on the available data. That is a fair assumption since the fire resistance of a system in the same way as its cost, is directly proportional to its protection thickness. The fire protection system developed in the framework of this research is referred as the plug-and-play system.

The consideration of unit cost is an indicative basis for the comparison of fire protection systems. Nevertheless, it must be noted that the surfaces or the areas to be protected by the different system is not always identical. Fig. 30 illustrates box- and actual areas for I an H steel sections exposed to fire. Box area Ap must be considered when protected with boards and plug-and-play systems, while actual area Am must be considered when protected with intumescent paints or sprays. Box- and actual areas are identical for hollow square steel sections.

A comparison of the four fire protection systems when applied on a 3 m high HEB300 steel profile is detailed in Table 19. Box- and actual areas for a 3 m high HEB300 steel profile were found to be equal to 3.60 m^2 and 5.19 m^2, respectively. Therefore, by multiplying the unit cost of each system with the appropriate area exposed to fire, actual cost ranges could be defined and allowed an unbiased cost comparison between the different systems. It can be observed that the plug-and-play system appear to be competitive compared with intumescent paints, while sprays and boards systems remain less expensive solutions. However, it must be recalled that aesthetic aspects are not the same for the four protections systems and that comparison is based on direct costs only.

Table 17
Direct cost details of the plug-and-play system.

Item	Value	Unit
15 mm thick rock wool board	10	[€/m^2]
30 mm thick rock wool board	22	[€/m^2]
Glue	2	[€/m^2]
Steel sheet	16	[€/m^2]
Material cost	**50**	**[€/m^2]**
Installation time for 2 workers	0.25	[h/m^2]
Manufacturing time for 1 worker	0.5	[h/m^2]
Average hourly labour costs	27	[€/h]
Worker Cost	**27**	**[€/m^2]**
Direct cost	**77**	**[€/m^2]**

Table 18
Unit cost for different fire protection systems.

Fire protection systems	Unit cost [€/m^2]			
	R30	R60	R90	R120
Intumescent paints	15–28	38–60	65–100	92–140[a]
Sprays	18–28	20–35	25–40	30–45[a]
Boards	20–40	30–55	40–65	50–75[a]
Plug-and-play	–	–	–	77

[a] Unit cost estimated by linear extrapolation.

Indirect costs of a fire protection refer to the costs generated within a construction project due to application of the protection on site. Since these costs are not related to the fire protection itself, they are often unconsidered when solutions are compared by fire design stakeholders. Indirect costs are usually quantified in terms of site delay and damage which have to be covered by the construction project. Fire protections requiring important installation time on site are more likely to generate delays and represent longer risk exposure for technicians. That is the case for boards, sprays and paints when applied on site. Particularly, sprays and intumescent paints can significantly impact the accessibility to a construction site area because they are wet applications and require a drying period.

Maintenance of the fire protection is also an important aspect of indirect costs. These costs are not straightforward to evaluate for the different systems due to the lack of data. However, it is important to mention that the plug-and-play system seldom requires maintenance thanks to the fact that the only components that could get damaged, i.e. the rock wool boards, are protected by the surrounding steel sheet. The main maintenance requirement that could be considered is the complete replacement of one plug-and-play system due to an accidental blow which would cause high deformations in the connection claws and could impact on the insulation efficiency of the protection. Therefore, had the maintenance costs been properly compared between the different fire protection systems, the ones related to the plug-and-play system would have been among the smallest.

Eventually, by considering direct and indirect costs, the plug-and-play protection system developed in this work constitutes a cost-effective solution.

8. Conclusions

This paper presented the development of an innovative and cost-efficient plug-and-play fire protection system for steel columns made of rock wool covered by a steel sheet. The connection system is based on bent steel sheets forming connection claws. Small-scale experimental tests were performed in an early stage of the protection design to evaluate its thermo-mechanical behaviour and its thermal insulation efficiency. Small-scale tests provided conclusive results regarding the plug-

Fig. 30. Area exposed to fire: a) Box area A_p; b) Actual area A_m.

Table 19
Cost comparison of fire protection systems applied on a 3 m high HEB300 steel profile.

Fire protection systems	Unit cost [€/m^2]	Area [m^2]	Actual cost [€]
Intumescent paints	92–140	5.19	477–726
Sprays	30–45	5.19	156–233
Boards	50–75	3.60	180–270
Plug-and-play	77	3.60	277

and-play system since no opening of connection claws was observed out of the seven specimens. A detailed 3D numerical model developed with the software ABAQUS showed the same observations, i.e. no connection claws opening after 120 min of exposure to standard fire. Then, 2D thermal numerical models developed with the finite element software SAFIR were calibrated against experimental results. Subsequently the analytical model prescribed in Eurocode 3 was adopted to verify the results of 2D thermal models. Both numerical and analytical models were in line and predicted similar steel temperature evolution with time. Consequently, these models served for the proper definition of the large-scale experimental campaign performed in the fire laboratory at the University of Liège. Large-scale tests aimed at evaluating five specimens to certify a single version of the fire protection according to the standard of regulation EN 13381-4 and allowed therefore its application in Europe. Thermal results obtained with large scale tests were finally found to be better than predictions based on calibrated models built on the small-scale test results. Indeed, mean temperatures of unloaded specimens were between 15% and 25% lower than the ones predicted after 120 min of exposure to standard fire. That showed the good outcomes of the optimisation process and the thermal efficiency of the developed fire protection. Furthermore, the large-scale experimental campaign namely allowed the thermo-mechanical evaluation of the protection system when equipped around a 3.1 m high steel HEM 220 column loaded to 60% of its vertical bearing capacity. The specimen survived 120 min of exposure to the standard fire. Additionally, a cost analysis of the plug-and-play protection system and a cost comparison with existing solutions demonstrated the cost-efficiency of the developed protection in terms both of direct and indirect costs. Eventually the plug-and-play fire protection system must be manufactured using steel sheets with a minimal thickness of 0.7 mm and with a rockwool thickness of 45 mm composed of two layers (15 mm + 30 mm). This system is certified to protect steel profiles presenting 'H', 'I' and hollows sections with box section factors going from 42 m^{-1} to 103 m^{-1}, by maintaining steel temperature below 550 °C for 120 min of exposure to standard fire.

Future perspectives will be addressed to investigate the behaviour of the fire protection exposed to natural fires and to non-uniform heating. In particular, the effects of significant thermal gradients on the claws will be studied.

Author Statement

Jérôme Randaxhe: Methodology, Writing - Original Draft, Software, Investigation, Formal analysis, Validation. Nicoleta Popa: Supervision, Project administration, Funding acquisition. Olivier Vassart: Supervision, Project administration, Conceptualization. Nicola Tondini: Conceptualization, Methodology, Writing - Review & Editing, Supervision.

Declaration of competing interest

The authors declare that they have no known competing financial interests or personal relationships that could have appeared to influence the work reported in this paper.

Acknowledgments

The development the fire protection system was entirely funded by the European commission through the XP-Resilience project and the grant agreement number 721816. ROCKWOOL® provided for free the rockwool board used in the specimens manufacturing. Small-scale experimental tests campaign was achieved in the metallurgy research centre CRM in Liège (Belgium). Large-scale experimental tests were achieved in the fire laboratory at the University of Liège (Belgium). All of them are gratefully acknowledged.

References

[1] M.K. Islam, M.J. Hasan, T. Manzur, Behavior of typical steel column sections under standard fire, in: International Conference on Disaster Risk Management, 2019.
[2] International Organization for Standardization, Fire Resistance Test – Elements of Building Construction – Part 1: General Requirements ISO/FDIS 834-1, 1999. Geneva.
[3] L. Petukhovskaia, Passive Fire Protection Methods of Load-Bearing Structures in Case of Hydrocarbon Fire, Saimaa University of Applied Sciences, 2018.
[4] H. Leborgne, L. Thomas, Techniques de protections rapportées des structures en acier, Constr. Met. (CTICM) 3 (1999) 123–135.
[5] National Institute of Standards and Technology - NIST, Fire Protection of Structural Steel in High-Rise Buildings, 2004.
[6] A. Lucherini, C. Maluk, "Intumescent coatings used for the fire-safe design of steel structures : a review, J. Constr. Steel Res. 162 (2019) 105712.
[7] D. De Silva, A. Bilotta, E. Nigro, Experimental investigation on steel elements protected with intumescent coating, Construct. Build. Mater. 205 (2019) 232–244.
[8] D. de Silva, A. Bilotta, E. Nigro, Approach for modelling thermal properties of intumescent coating applied on steel members, Fire Saf. J. 116 (June) (2020) 103200.
[9] G.J. Griffin, The Modeling of heat transfer across intumescent polymer coatings, J. Fire Sci. 28 (2010) 249–277.

[10] B. Gardelle, S. Duquesne, P. Vandereecken, S. Bourbigot, Resistance to fire of silicone-based coatings : fire protection of steel against cellulosic fire, J. Fire Sci. (2014) 374–387.
[11] P. Luangtriratana, B.K. Kandola, S. Duquesne, S. Bourbigot, Quantification of thermal barrier efficiency of intumescent coatings on glass fibre-reinforced epoxy composites, Coatings (2018) 1–18.
[12] C. Chen, J. Zeng, B. Shen, Experimental Investigation on Performance of Intumescent Coating for Steel Plate at Elevated Temperature, vol. 22, Cent. South Univ. Press, 2015, pp. 3151–3158.
[13] T. Mariappan, Recent developments of intumescent fire protection coatings for structural steel : a review, J. Fire Sci. 34 (2) (2016) 120–163.
[14] G.E. Fulmer, Method of Making a Fire-Retardant Product Having a Foamed Lore and a Fire-Retardant Protective Layer, 1982. US 4349494.
[15] Q. Zhang, V.C. Li, Development of durable spray-applied fire-resistive engineered cementitious composites (SFR-ECC), Cement Concr. Compos. 60 (2015) 10–16.
[16] X. Zhang, L. Peng, Z. Ni, T. Ni, Y. Huang, Y. Zhou, Experimental study on the fire performance of tubular steel columns with membrane protections for prefabricated and modular steel construction, Materials (2018) 1–12.
[17] P. Keerthan, M. Mahendran, Numerical studies of gypsum plasterboard panels under standard fire conditions, Fire Saf. J. 53 (2012) 105–119.
[18] S. Gottfried, Fire and Heat Protection Wrap for Structural Steel Columns, Beams and Open Web Joists, 2001. WO 01/72506 A1.
[19] D. Zago, R. Keiser, Covering and Fire Protection Device for Metal Girders, 2011. WO 2011/045247 A1.
[20] A.S. Parker, Plasterboard to Column Clip, 1973. US 3748815.
[21] P.P. Ramos, Fire Protection System for Wide Flange Steel Columns and Beams, 2013. US 2013/0167475 A1.
[22] O. Akaa, A. Abu, M. Spearpoint, S. Giovinazzi, Optimising design decision-making for steel structures in fire using a hybrid analysis technique, Fire Saf. J. 91 (February) (2017) 532–541.
[23] O.U. Akaa, A. Abu, M. Spearpoint, S. Giovinazzi, A group-AHP decision analysis for the selection of applied fire protection to steel structures, Fire Saf. J. 86 (March) (2016) 95–105.
[24] J.W. Lim, T. Baalisampang, V. Garaniya, R. Abbassi, F. Khan, J. Ji, Numerical analysis of performances of passive fire protections in processing facilities, J. Loss Prev. Process. Ind. 62 (September) (2019) 1–12.
[25] European Committee for Standardization CEN, Eurocode 3: Design of Steel Structures – Part 1–2: General Rules – Structural Fire Design. EN 1993-1-2, European Commitee for Standardization, CEN, Brussels, 2005.
[26] European Committee for Standardization CEN, Test Methods for Determining the Contribution to the Fire Resistance of Structural Members – Part 4 : Applied Passive Protection to Steel Members Contents, 2011, pp. 1–85.
[27] W. Wang, G. Li, Fire-resistance study of restrained steel columns with partial damage to fire protection, Fire Saf. J. 44 (8) (2009) 1088–1094.
[28] ROCKWOOL, Conlit Steelprotect Board - Technical Specifications [Online]. Available, https://fr.rockwool.be/produits/isolation-technique/applications-ignifuges/conlit-steelprotect-board/#Tools&Downloads. (Accessed 26 February 2020).
[29] KUHN, "Kerafix ® Fxl 200," *KUHN - Fire Protection Materials*, 2016, p. 11 [Online]. Available, https://kuhn-brandschutz.com/content/uploads/TDS_ROKU_KERAFIX-FXL-200_EN.pdf. (Accessed November 2020).
[30] Dassault Systemes, ABAQUS - Software for Nonlinear Finite Element Analysis, 2016 [Online]. Available, https://www.simuleon.com/simulia-abaqus/abaqus-standard/. (Accessed 26 February 2020).
[31] J.-M. Franssen, T. Gernay, Modeling structures in fire with SAFIR®: Theoretical background and capabilities, J. Struct. Fire Eng. 8 (3) (2017) 300–323.
[32] J.-B. Schleich, Implementation of Eurocodes - Handbook 5 - Design of Buildings for the Fire Situation, *Leonardo da Vinci pilot project*, Luxembourg, 2005.
[33] European Committee for Standardization CEN, Eurocode 3: Design of Steel Structures – Part 1-1: General Rules and Rules for Buildings. EN 1993-1-1, European Committee for Standardization CEN, Brussels, 2005.
[34] EMFI, ISOLEMFI 3300- Technical Specifications, 2018 [Online]. Available, http://www.emfi.com/en/produits/products.html?cp=50040A. (Accessed 26 February 2020).
[35] ArcelorMittal, ArcelorMittal Construction Products, 2017 [Online]. Available, www.arcelormittalconstruction.be. (Accessed 27 February 2020).
[36] E. Charlton, Where Labour Costs the Most (And Least) in the European Union, *World Economic Forum*, 2019 [Online]. Available, https://www.weforum.org/agenda/2019/05/chart-labour-costs-in-european-union. (Accessed 27 February 2020).
[37] BauforumStahl, Kosten im Stahlbau 2019 Basisinformationen zur Kalkulation/Steel construction costs 2019 - Basic information about calculation, *CEEC - European Council of Construction Economists*, 2019 [Online]. Available, https://bauforumstahl.de/fileadmin/user_upload/bauforumstahl.de/wirtschaft-und-politik/baukosten/Kosten_im_Stahlbau_2019v2.pdf. (Accessed 26 February 2020).